The DOI for this manuscript is doi: 10.1175/BAMS-D-14-00272.1

Pan, L., E. Atlas, R. Salawitch, S. Honomichl, J. Bresch, W. Randel, E. Apel, R. Hornbrook, A. Weinheimer, D. Anderson, S. Andrews, S. Baidar, S. Beaton, T. Campos, L. Carpenter, D. Chen, B. Dix, V. Donets, S. Hall, T. Hanisco, C. Homeyer, L. Huey, J. Jensen, L. Kaser, D. Kinnison, T. Koenig, J. Lamarque, C. Liu, J. Luo, Z. Luo, D. Montzka, J. Nicely, R. Pierce, D. Riemer, T. Robinson, P. Romashkin, A. Saiz-Lopez, S. Schauffler, O. Shieh, M. Stell, K. Ullmann, G. Vaughan, R. Volkamer, and G. Wolfe, 2016: The Convective Transport of Active Species in the Tropics (CONTRAST) Experiment. Bull. Amer. Meteor. Soc. doi:10.1175/BAMS-D-14-00272.1, in press.

The Convective Transport of Active Species in the Tropics (CONTRAST) Experiment

L. L. Pan[1], E. L. Atlas[2], R. J. Salawitch[3], S. B. Honomichl[1], J. F. Bresch[1], W. J. Randel[1], E. C. Apel[1], R. S. Hornbrook[1], A. J. Weinheimer[1], D. C. Anderson[3], S. J. Andrews[4], S. Baidar[5], S. P. Beaton[1], T. L. Campos[1], L. J. Carpenter[4], D. Chen[6], B. Dix[5], V. Donets[2], S. R. Hall[1], T. F. Hanisco[7], C. R. Homeyer[8], L. G. Huey[6], J. B. Jensen[1], L. Kaser[1], D. E. Kinnison[1], T. K. Koenig[5], J-F Lamarque[1], C. Liu[9], J. Luo[1,#], Z. J. Luo[10], D. D. Montzka[1], J. M. Nicely[3], R. B. Pierce[11], D. D. Riemer[2], T. Robinson[12], P. Romashkin[1], A. Saiz-Lopez[13], S. Schauffler[1], O. Shieh[12], M. H. Stell[1,14], K. Ullmann[1], G. Vaughan[15], R. Volkamer[5], G. Wolfe [7,16]

[1]National Center for Atmospheric Research, Boulder, Colorado, USA
[2] University of Miami, Florida, USA
[3]University of Maryland, College Park, Maryland, USA
[4]University of York, York, UK
[5]University of Colorado Boulder, Boulder, Colorado, USA
[6]Georgia Institute of Technology, Atlanta, Georgia, USA
[7]NASA Goddard Space Flight Center, Greenbelt, Maryland, USA
[8]University of Oklahoma, Norman, Oklahoma, USA
[9]Texas A&M University at Corpus Christi, Texas, USA
[10]City College of New York, New York, New York, USA
[11]NOAA Satellite and Information Service (NESDIS) Center for Satellite Applications and Research (STAR), Madison Wisconsin, USA
[12]University of Hawaii at Mānoa, Hawaii, USA
[13]Institute of Physical Chemistry Rocasolano, CSIC, Madrid, Spain
[14]Metropolitan State University, Denver, Colorado, USA
[15]University of Manchester, Manchester, UK
[16]University of Maryland Baltimore County, Baltimore, Maryland, USA
[#]Now at Lanzhou University, Lanzhou, China

Contact information of the corresponding author:
Laura L. Pan,
National Center for Atmospheric Research
P.O. Box 3000, Boulder, CO 80307-3000
Email: liwen@ucar.edu
Phone: 303-497-1467

Submitted to *Bulletin of the American Meteorological Society*, September 30, 2015

Revised February 18, 2016

Capsule

Airborne observations over the tropical western Pacific warm pool characterize the role of tropical convection in linking oceanic processes to ozone chemistry in the upper troposphere and lower stratosphere

Abstract:

The Convective Transport of Active Species in the Tropics (CONTRAST) experiment was conducted from Guam (13.5° N, 144.8° E) during January-February 2014. Using the NSF/NCAR Gulfstream V research aircraft, the experiment investigated the photochemical environment over the tropical western Pacific (TWP) warm pool, a region of massive deep convection and the major pathway for air to enter the stratosphere during Northern Hemisphere (NH) winter. The new observations provide a wealth of information for quantifying the influence of convection on the vertical distributions of active species. The airborne in situ measurements up to 15 km altitude fill a significant gap by characterizing the abundance and altitude variation of a wide suite of trace gases. These measurements, together with observations of dynamical and microphysical parameters, provide significant new data for constraining and evaluating global chemistry climate models. Measurements include precursor and product gas species of reactive halogen compounds that impact ozone in the upper troposphere/lower stratosphere. High accuracy, in-situ measurements of ozone obtained during CONTRAST quantify ozone concentration profiles in the UT, where previous observations from balloon-borne ozonesondes were often near or below the limit of detection. CONTRAST was one of the three coordinated experiments to observe the TWP during January-February 2014. Together, CONTRAST, ATTREX and CAST, using

complementary capabilities of the three aircraft platforms as well as ground-based instrumentation, provide a comprehensive quantification of the regional distribution and vertical structure of natural and pollutant trace gases in the TWP during NH winter, from the oceanic boundary to the lower stratosphere.

1. Introduction and Scientific Motivation

The tropical western Pacific (TWP) warm pool is a uniquely important region for the earth's climate system. The warm pool, often defined by sea surface temperature (SST) in excess of 28 °C (Wyrtki, 1989), is the largest source of latent heat release and water vapor into the atmosphere, and the center of action for the El Niño-Southern Oscillation (ENSO) (Webster and Lukas, 1992). Fueled by the warm sea surface, the region has intense and massive deep convection and precipitation (Liu and Zipser, 2015). At the upper troposphere/lower stratosphere (UTLS) level, strong upwelling during the northern hemisphere (NH) winter season couples to the deep convection to make the TWP region the largest source for tropospheric air entering the stratosphere (Newell and Gould-Stewart, 1981; Fueglistaler et al., 2004; Krüger et al., 2008; Bergman et al., 2012). This is also the region of coldest temperatures in the Tropical Tropopause Layer (TTL) during NH winter (Fueglistaler et al., 2009; Randel and Jensen, 2013); therefore it plays a critical role in controlling the amount of water vapor that enters the lower stratosphere (Newell and Gould-Stewart, 1981; Holton and Gettelman, 2001; Schoeberl et al., 2011). The effect of dehydration in the region is reflected in satellite cloud observations, which show that the

region has the largest fraction of high clouds (17-18 km level) (e.g., Yang et al., 2010) and significant occurrence of clouds above the tropopause (Pan and Munchak, 2011).

The unique thermal and dynamical behaviors of this region also create a special chemical environment. A number of field studies and satellite data have identified extremely low O_3 in the region, near or below the detection limit of typical ozonesondes. This is especially true at the TTL level where measurements of O_3 below 20 ppbv suggest a major contribution of convectively lifted air from the oceanic boundary layer (e.g., Kley et al., 1996; Crawford et al., 1997; Thompson et al., 2011; Rex et al., 2014). This low ozone environment may have an impact on the abundance of hydroxyl radical (OH) in the troposphere, which is a significant agent for self-cleaning of the atmosphere. Deep convection connects emissions from oceanic biological processes to the UTLS. Thus, the UTLS over the oceanic warm pool region is expected to have elevated concentrations of organic halogen species such as dibromomethane (CH_2Br_2), bromoform ($CHBr_3$) and methyl iodide (CH_3I). These compounds are significant contributors to the input of reactive bromine and iodine into the mid to upper tropical troposphere where they, along with their inorganic breakdown products, represent an important component of the natural background ozone budget (Saiz-Lopez et al., 2012; Wang et al., 2015). These short-lived halogens and their inorganic oxidation products may have additional impacts on stratospheric chemistry (Salawitch et al., 2005; Fernandez et al., 2014; Saiz-Lopez et al., 2015). Our measurements in the TWP were designed to address current uncertainties in both the halogen-mediated loss of ozone in the UTLS as well as the budget and partitioning of reactive halogen inputs to the stratosphere.

Recognizing the importance of the TWP region, a number of large-scale field experiments have been conducted to investigate a range of atmospheric dynamics and chemistry questions. Ocean-atmosphere coupling was the focus of Tropical Ocean – Global Atmosphere Coupled Ocean Atmosphere Response Experiment (TOGA-COARE) (1988), which deployed large arrays of soundings and collected measurements from multiple aircraft (Webster and Lukas, 1992). The NASA Global Tropospheric Experiment (GTE) program conducted a series of airborne studies using the DC-8 aircraft and obtained detailed chemical information over the tropical Pacific, including the warm pool region (e.g., Hoell et al., 1999) up to 12 km altitude. The Biomass Burning and Lightning Experiment (BIBLE) campaign, using a Gulfstream II research aircraft, focused on the impact of lightning and biomass burning emissions of aerosols and trace gases on ozone chemistry (Kondo, et al., 2002). Despite these studies, the impact of convection on chemistry in the warm pool region has not previously been well characterized, especially at the TTL level (13-17 km). Figure 1 shows the climatological location of the warm pool in the NH winter season and locations of ozonesonde launch sites, which indicate the lack of ozone measurements in the core of the warm pool. The lack of adequate observations of trace gas composition, including ozone and reactive halocarbons, in the warm pool region leaves a significant gap in our understanding of the chemistry within the TTL and the transport into stratosphere over the TWP.

A broad range of scientific objectives motivated the coordination of three airborne experiments for research over the TWP warm pool. The objectives required aircraft with the appropriate instrument payloads that could cover altitudes from the marine boundary layer (MBL) to the lower stratosphere (LS). The major objectives addressed by the three

aircraft complement include better understanding the role of deep convection in coupling the MBL to UTLS chemical composition, characterization of the processes controlling water vapor and short-lived chemical species transported into the stratosphere, definition of the abundance and partitioning of halogen species and their impact on UTLS ozone, and evaluation of the chemical coupling of ocean and atmospheric oxidation capacity in the warm pool region. The experiments were all based in Guam (13.5° N, 144.8° E) with research flights conducted during January and February 2014. The Airborne Tropical Tropopause Experiment (ATTREX) used the high-altitude NASA Global Hawk (GH) to sample chemical and microphysical parameters at altitudes between ~14-18 km (see ATTREX overview by Jensen et al., this issue). The Coordinated Airborne Studies in the Tropics (CAST) experiment used the UK FAAM BAe 146 research aircraft to measure a large suite of chemical tracers from the MBL up to ~7 km altitude (see CAST overview by Harris et al., this issue). The CONTRAST experiment used the NSF/NCAR Gulfstream V (GV) research aircraft to sample a wide variety of chemical species from the MBL to ~ 15 km. The concept of the coordinated campaigns is illustrated in Figure 2.

This article provides an overview for the CONTRAST experiment, including discussions of scientific synergy with the other two coordinated experiments. Within the context of the coordinated campaigns, the main scientific objectives of the CONTRAST experiment were:

- Characterizing the influence of deep convection on the chemical composition and the photochemical budget of O_3 at the level of convective outflow over the western Pacific
- Evaluating the budget of organic and inorganic bromine and iodine in the TTL
- Investigating transport pathways from the oceanic surface to the tropopause using coordinated flights with CAST BAe-146 and ATTREX GH

149 This overview presents the design and implementation of the CONTRAST experiment, the
150 background information for using CONTRAST data, and selected scientific and operational
151 highlights. These highlights are chosen to promote new research opportunities that
152 CONTRAST data may enable. The description of the operation and facility may also serve
153 as a useful reference for future field campaign planning.

154 ## 2. Meteorological Setting of the Experiment

155 Located at the northern edge of the warm pool near the division of rising and sinking
156 branches of the Hadley cell in the NH winter season, Guam was an ideal base for the
157 campaign. The GV flights from Guam have access to areas of active convection (to the
158 south) and to the subtropical jet stream (to the north). Furthermore, the flight operations
159 and instrument maintenance were less challenging since the island was in its dry season,
160 and excellent logistical support for airborne operations was available on Guam.

161 Figure 3 shows the distribution of the 12-14 km cloud fraction from CloudSat data, together
162 with additional key dynamical elements important to the Guam operational domain. The
163 wind direction and the geopotential height (GPH) indicate that, over the region of
164 persistent deep convection, the upper tropospheric flow is dominated by a large-scale
165 anticyclonic pattern that is symmetrically distributed with respect to the convective axis
166 (Dima and Wallace, 2007). The GV nominal operational range is represented in Figure 3 by
167 the circle of 1500 nautical miles (nmi) radius. An additional circle of 1000 nmi radius is
168 shown in Figure 3 to indicate the range when planning extensive loitering was considered
169 in the flight plan. The northern part of the research domain includes an intense jet stream,
170 illustrated by contours of wind speed greater than 50 m/s. The jet core marks the

dynamical division of the tropics and extratropics. The increase of potential vorticity (PV) near the jet indicates the rapid change of air mass character from tropospheric to stratospheric at UTLS levels.

Winter 2014 was characterized as ENSO-neutral with a Niño index of about −0.5 (NOAA CPC, http://www.cpc.ncep.noaa.gov/products/analysis_monitoring/enso_disc_mar2014/). SST anomalies over the Western Pacific were slightly positive (+1 °C) between 0 and 10 °N during January and February on the northern side of the climatological warm pool. The equatorial trough was a common feature in low latitudes during the period with a few periods of enhanced low-level convergence over the study region. Two significant Madden-Julian Oscillation (MJO) events occurred during the study period. The first, during the second half of January, was accompanied by the formation of tropical storms Lingling and Kajiki near the Philippines. These storms may have helped Guam receive near-record January rainfall. The second MJO event occurred in late February and was accompanied by the formation of Typhoon Faxai, which was located mostly east of Guam (145 °E). Repeated cold fronts/shear lines moved from the north to Guam's latitude during early 2014, which enhanced surface northeasterlies and promoted low-level convergence and precipitation.

3. Design and Operation of the Experiment

3.1 Platform and Payload

The base in Guam coupled with the range and duration of the NSF/NCAR Gulfstream V (GV) aircraft allowed sampling from MBL to the lower TTL, including the level of the main convective outflow (12-14 km) in the warm pool region. With the CONTRAST payload and aircraft configuration, the GV typically flew at flight altitudes between 13-14 km with a

193 flight ceiling near 15 km (~48,000 feet in pressure altitude). Figure 4 and Table 1
194 summarize the GV payload configuration during the CONTRAST experiment.
195 To meet the scientific objectives of the CONTRAST mission, the GV payload was designed to
196 characterize the chemical and photochemical environment of TWP at all altitudes,
197 especially the level of convective outflow. The instrument payload had sensors for various
198 trace gases, aerosols, and radiation. The trace gas measurements were aimed at gases with
199 different sources, atmospheric trends, and chemical lifetimes. These trace gas properties
200 allowed an examination of long range and convective transport and chemical reactivity in
201 the CONTRAST region.

202 To measure organic halogen composition, the payload included a combination of the
203 Advanced Whole Air Sampler (AWAS), a canister sampling system, the Trace Organic Gas
204 Analyzer (TOGA), an *in situ* online gas chromatograph/mass spectrometer (GC/MS), and
205 fast-response instrumentation for CO, CO_2, and CH_4. The TOGA and AWAS provide
206 complementary measurements of trace gases. TOGA measured approximately 75 volatile
207 organic compounds (VOCs), including C_3-C_8 nonmethane hydrocarbons (NMHC),
208 halocarbons, organic nitrates, and several C_1-C_4 oxygenated VOC (OVOC) (Apel et al., 2015).
209 The AWAS measured a full suite of NMHC, halocarbons, and organic nitrates at high
210 precision but with lower spatial resolution compared to TOGA. A number of trace gases
211 measured by both systems provided good overlap for data comparison and complementary
212 sampling. In addition, whole air samplers were deployed on all three aircraft (see Jensen et
213 al. and Harris et al., this issue) and provide a consistent dataset from the MBL to the LS (see
214 Figure 9 in section 4).

Measurements of radiation and relevant reactive gases provided data to define the photochemical environment of the tropical UT, to examine the impact of convective inputs on ozone chemistry, and to evaluate inorganic halogenated products produced from organic precursors. These measurements included actinic flux, ozone, formaldehyde, nitric oxide and nitrogen dioxide (or NO_x, the sum of the pair), and halogen radical species. The NO_x measurements also provided information on the input of lightning-produced nitric oxide in this area of deep convection.

To evaluate the budget and partitioning of bromine in the TTL, organic bromine precursors were measured by AWAS and TOGA. Selected inorganic bromine species were measured in situ by chemical ionization mass spectrometry (CIMS) (Huey, 2007), and remote sensing Airborne Multi AXis Differential Optical Absorption Spectroscopy (AMAX-DOAS) (Baidar et al., 2013; Volkamer et al., 2015). In addition, iodine oxide (IO) was measured by AMAX-DOAS (Dix et al., 2013; Volkamer et al., 2015). The AMAX-DOAS and CIMS data also provide a link to comparable measurements on the GH and BAe-146 aircraft. Finally, the payload also included cloud and aerosol measurements for determining aerosol size distributions and for evaluating heterogeneous chemical processing.

3.2 Research Flights

A total of 16 GV research flights were made during the CONTRAST campaign including 3 transit flights and 13 local flights conducted in Guam. The ground tracks of these flights are shown in Figure 5. The Guam based flights sampled latitudes between 20°S and 40°N and altitudes between ~100 m and ~15 km above sea level (see flight tracks in altitude-latitude space in Figure 11). Extensive vertical sampling of the atmosphere in the study region

237 resulted in more than 100 complete profiles during the campaign. These profiles include
238 the eastern and the central Pacific, but most were conducted in the TWP.

239 The research flights were planned according to seven scenarios, each designed to meet a
240 set of observational objectives:

241 1. Domain survey (RF01-04, RF07, RF14): this type of flight was designed to map out
242 the background distributions and gradients of compounds of different lifetimes and
243 source/sink distribution. Gradients include those from the eastern to western
244 Pacific, as well as those within the Guam domain. This type of flight typically
245 covered the largest sampling range, including excursions out of the nominal domain.
246 2. Fresh convective outflow (RF05, RF09-12, RF14): this type of flight was designed to
247 sample the outflow of ongoing convection and to contrast the enhancement of short-
248 lived species within outflow to the upper tropospheric background, that is
249 influenced by more aged convection as well as long-range transport.
250 3. Dawn/dusk (RF08, RF13): this type of flight was designed to investigate
251 photochemical evolution and halogen partitioning that occurs during the transition
252 from daylight to darkness and vice versa. The strategy was to sample the same air
253 mass through the period of solar zenith angle change. To accomplish this, the center
254 of anticyclonic flow was targeted as a relatively stagnant air mass for chemical
255 characterization and photochemical evolution.
256 4. Stratospheric survey (RF06, RF15): this type of flight was designed to sample the
257 northern part of the domain to contrast the chemical composition of the tropical UT
258 with that of the extratropical LS.

5. Dynamical boundaries and structures (RF06, RF10, RF14): these flights were special surveys conducted in response to the presence of dynamical boundaries in the flight domain, such as a shear line and a crossing of the ITCZ. The goal was to characterize the role of these dynamical structures as physical boundaries to chemical composition.
6. Ozonesonde co-location (RF09, RF11, RF12, RF14): these flights involved a segment of sampling over Guam or Manus Island (2° S) when there was a coincident ozonesonde launch from the ATTREX or CAST team. The comparison over Manus was particularly important, since ozonesonde calibration issues are challenging in the convectively influenced TTL (Newton et al, 2016).
7. BAe-146 or Global Hawk coordination (RF08, RF11, RF12): this type of flight involved two or three aircraft flying on the same day, sampling a geographic region close to the same time. The coordinated flights between the GV and the BAe146 were typically designed to have a segment of "repeated track", in which the same region and altitude was sampled by the two aircraft sequentially with a short time separation to allow for instrument comparisons.

Table 2 provides a brief summary of the research flights with relevant flight scenarios noted by numbers. As shown in the table, often more than one scenario was involved for a given flight. The table also shows the flight information regions (FIRs) within which each research flight was conducted. The GV operated in the Oakland Oceanic FIR (USA) for the majority of the flight hours. Flight operations in other FIRs (Fukuoka FIR (Japan) and Port Moresby FIR (Papua New Ginnea)) were more difficult due to numerous issues. An example was discussed in section 4.5.

3.3 Forecasting tools and platform

CONTRAST flight planning and forecasting employed a suite of models that covered the range of dynamical and chemical processes relevant to the science goals. NCEP's Global Forecast System (GFS) and NCAR's Weather Research and Forecasting (WRF) community model aided the meteorological forecasts for CONTRAST. The 0.5° GFS pressure-level data files were used to produce 5-day forecast plots at 6-hour increments and were made available in the project's Field Catalog (described below). The Advanced Research WRF (ARW, Skamarock et al. 2008) was run in real-time at the NCAR/Wyoming Supercomputing Center to provide a more detailed 72-hour forecast of moist convection, clouds, and winds over the study region. The ARW was configured in a 15-km, 40-level grid covering much of the western Pacific with a 3-km nested grid.

Chemical forecasting was an important part of flight planning. CAM-chem, a global chemistry-climate model (Lamarque et al., 2012) run in the specified dynamics mode (i.e., nudged by observed winds, hereafter referred to as CAM-chem-SD), was run operationally during the CONTRAST field phase to provide 72-hour chemical forecasts for mission planning. The model was configured in 1×1 degree horizontal resolution with 56 levels from the surface to 2 hPa and used in its specified-dynamics configuration, driven with NASA GMAO/GEOS-5 meteorological fields. T he model chemistry includes a detailed representation of tropospheric and stratospheric chemistry (~180 species; ~500 chemical reactions), including very short-lived (VSL) halogens (details are found in Fernandez et al., 2014 and Saiz-Lopez et al., 2014). The model routinely forecast distributions of trace gas species including ozone, hydroxyl radical (OH), nitrogen oxides ($NO_x = NO+NO_2$), carbon monoxide (CO), bromine oxide (BrO), iodine oxide (IO), and VSL organic halogens, e.g.,

bromoform ($CHBr_3$), dibromomethane (CH_2Br_2), and methyl iodide (CH_3I). This combination of species assisted the science team in flight planning that could, for example, delineate aged versus more recently polluted air masses, identify areas of stratospheric intrusions, or target air that had been recently lofted by convection.

In addition to CAM-chem-SD, the Real-time Air Quality Modeling System (RAQMS) (Pierce et al., 2007) and the Monitoring Atmospheric Composition & Climate (MACC) (Flemming et al., 2009), both of which assimilate global satellite data, provided complementary chemical forecast information. In particular, RAQMS provided a number of additional short-lived MBL tracers, such as dimethyl sulfide (DMS) and methyl ethyl ketone (MEK) during the campaign. The MACC forecast assimilated comprehensive global observations of chemical composition combined with the ECMWF meteorological forecasting system. MACC provided plots for the operation domain of O_3, CO, CH_4, NO_x, black carbon, HCHO, OH, NO, NO_2, OH, and HO_2 and provided comparisons to the CAM-chem-SD forecasts of chemical fields.

Figure 6 shows forecast plots for RF10 as an example, where the CAM-chem-SD forecasted a "CO river" that was primarily a biomass burning plume from southeast Asia transported by the jet stream to the Guam region, and the WRF model successfully forecast the presence of the ITCZ in the domain. Both the "CO river" and the ITCZ were successfully sampled in RF10. The former is further discussed in Section 4.4.

The large suite of forecast materials were integrated and documented on the NCAR EOL Field Catalog for the CONTRAST project (http://catalog.eol.ucar.edu/contrast). The Field

Catalog provided a virtual operations center that allowed team members to participate in the daily briefings, either in the field or from their home institutions. The Catalog also served to document the information flow during the experiment for future reference. In general, the forecast models provided good guidance for flight planning that allowed successful sampling of targeted meteorological and chemical features of interest. The main limitation of the forecast models (including the 3-km ARW simulations) was their difficulty in representing the observed evolution of convective systems over the low-latitude ocean regions. The experience and additional analyses by the forecasters were important in these cases.

3.4 Flight planning and operation.

A daily operations meeting was held in the CONTRAST operations center in Guam on most aircraft maintenance days. The daily meeting was a key step in gathering the science team's input for flight planning. Typically, different flight scenario options were discussed after the weather briefing and chemical forecast. The priority of different flight options was defined by the campaign science objectives, while meteorological conditions and chemical forecast dictated the practical possibilities of near term flight operations. Planning of the RF10 mission serves as a good example. After extensive team discussion, both pollution transport ("CO river", Fig. 6a) and the impact of dynamical structures on chemical composition (ITCZ, Fig. 6b) were included in the flight plan. Typically, a flight or no-flight decision for the next-day was made by the team by the end of the meeting.

Following the daily operations meeting in the morning, the Principal Investigators (PIs) and the operation center team would proceed with making an initial flight plan that was reviewed by the pilots, who filed the adjusted flight plan with the relevant air traffic control centers (ATCs). The plan was adjusted several hours before flight, if necessary, based on updated meteorological information from models and satellite imagery. The final flight plan was filed two hours before take-off.

3.5 Nowcasting and real time decision-making

Because of rapid development and uncertain movement of convective systems, nowcasting and real-time decision-making were an important part of flight operations. The near-real-time satellite images from MTSAT2 were essential for providing information on convection. The NCAR EOL Field Catalog Map and Mission Coordinator Map were visible to the flight scientist onboard the GV and also to mission support at the Operations Center. These maps were essential tools for real-time flight monitoring and decision-making. Figure 7 gives an example of the real-time display from the Field Catalog Map, which integrates the real-time aircraft position with the near real-time operational products. The display shows the real-time position of all three aircraft on 13 February 2014, near 04:00 UTC, and the location of the convective systems targeted by the GV. As indicated by the figure, this flight successfully sampled convective outflow from widespread active convection southwest of Guam. An example of trace-gas measurements from this flight will be shown in next section.

The flight on 13 February (RF11) also provided a good example of real-time flight plan adjustment. Initially the flight was planned to pass the convective region at different altitudes to sample the air above and within the convective outflow. The mission scientist requested flight level 43 Kft to be above the convection when the research aircraft entered the active region for the first pass. The altitude request was based on estimated altitude from the satellite IR image. During this segment, a 5 m/s updraft was sampled (see figure 8). The flight level for the second pass was requested at 37 Kft, but it was found to be too low (visually below the outflow cloud layer). The decision was made to request a third pass at 40 Kft, which resulted in the sampling of significant boundary layer tracer enhancement associated with a 13 m/s updraft (Figure 8). The ATC response time over the oceanic region with no radar was at least 15 to 20 minutes, which was reflected by the large loop of the GV flight track out of the convective region (Figure 7).

4. Scientific and Observational Highlights

4.1 Sampling convective outflow

One of the key observational objectives was sampling air masses in regions of active convective outflow, as well as nearby air masses not influenced by recent convection, to quantify the influence of convection on the composition of the TWP troposphere. Targeting active convection is a significant challenge for flight operations in general, but especially over oceanic domains such as the TWP because of the absence of ground-based weather radar coverage. Aided by the real-time information described in section 3, the GV succeeded in targeting active convection during multiple flights in CONTRAST.

Figure 8 shows an example of the impact of active convection on the chemical composition of the UT using data acquired during RF11 conducted on 13 February 2014. The figure shows a 3-hour segment of the flight, during which the GV sampled the same convective system (as shown in satellite IR map in Figure 7) three times at different altitudes. Convectively generated turbulence and the region of strong upward motion are indicated by the vertical wind velocity. Two time periods of active convection sampled are marked by the ~ 5 m/s (near 02:00 UTC) and the ~ 13 m/s (between 03:49 and 03:54 UTC) updraft events. Selected chemical species measured by the TOGA instrument demonstrate the strong impact of convection on the composition of UT air masses, indicated by the contrast of the air masses from inside to outside of convective outflow. The three selected species are all relatively short-lived with estimated lifetimes ranging from less than a day for acetaldehyde (Millet et al., 2010) and DMS (Langner and Rodhe, 1991) to days for MEK (e.g., Calvert et al., 2011). These species can all be produced by marine biological processes (Carpenter et al., 2010). They were all observed at elevated mixing ratios in the marine boundary layer during this flight. At the flight level of ~ 12 km, these species exhibit low mixing ratios characteristic of the background UT outside of the active convection region. The low background levels reflect the rapid decrease of their abundance with altitude. Significant enhancement was observed during both periods of sampling near a convective updraft. In the vicinity of the 13 m/s updraft, the mixing ratios show values only slightly less than in the boundary layer, indicating very little processing or mixing took place during transport of the air masses between the surface and the 12-km level.

4.2 Impact of convection on vertical distribution of VSL halocarbons

414 An important objective of CONTRAST was to quantify the abundance of the halogenated
415 VSL compounds throughout tropospheric column of the TWP. Bromine chemistry is
416 important for the photochemistry of O_3 in both the stratosphere and the tropical
417 troposphere (e.g., Ko et al. ,1997; Saiz-Lopez and von Glasow, 2012; Salawitch et al., 2005;
418 Frieler et al., 2006; Carpenter and Reimann, 2014). Additionally, measurements and
419 modeling suggest that halogen cycles involving both bromine and iodine could contribute
420 to chemical loss of O_3 in the tropical atmosphere (e.g., Saiz-Lopez et al. ,2012, 2015; Dix et
421 al., 2013; Carpenter et al., 2013; Volkamer et al., 2015; Wang et al., 2015), though we focus
422 just on bromine here.

423 Figure 9a shows the profile in the TWP of the total bromine content of the two most
424 important bromine-bearing VSL species, CH_2Br_2 and $CHBr_3$, using data from all three
425 aircraft. Detailed descriptions of the data and the result of inter-comparisons are given by
426 Andrews et al. (2015). These bromocarbons are produced by biological processes in the
427 tropical ocean and have lifetimes in the upper troposphere of ~ 17 days ($CHBr_3$) and ~ 150
428 days (CH_2Br_2) (Carpenter and Reimann, 2014). The measurements shown in Figure 9a
429 demonstrate the impact of convection on VSL bromocarbons and highlight the vertical
430 structure of total bromine that can be obtained by synergistic sampling conducted by three
431 aircraft. The profile displays a pronounced reverse "S" shape, with strong decrease above
432 the MBL and enhancement between 10 and 15 km altitude, which is a clear signature of
433 convective uplifting of MBL air. The layer of enhancement is largely consistent with the
434 peak in cloudiness as derived from the CloudSat cloud profiling radar (Figure 9b)
435 (Stephens et al., 2008). The vertical distribution of the cloud fraction serves as an
436 illustration of the convective outflow layer. Numerous details concerning the outflow (e.g.,

437 the level where maximum mass is detrained) can be obtained from analysis of the radar
438 profiles of the anvils, as discussed in Takahashi and Luo (2012). Hence, cloud radar and
439 VSL chemical compound measurements offer consistent and complementary views of the
440 deep convective outflow and transport in the TWP.

441 The amount of total VSL bromine at the tropopause (about 17 km) defines one pathway for
442 transport of bromine from VSL compounds to the stratosphere, termed Source Gas
443 Injection (SGI). The result in Figure 9a, when supplemented by the bromine content of
444 other VSL species such as $CHBr_2Cl$, CH_2BrCl, and $CHBrCl_2$ that will soon be available, will
445 represent the first experimental determination of SGI of bromine in the TWP. The other
446 route for stratospheric supply of bromine from VSL compounds, Product Gas Injection
447 (PGI), represents cross tropopause transport of inorganic species. The value of PGI will be
448 quantified by ATTREX measurements of BrO in the tropical lowermost stratosphere as well
449 as CONTRAST measurements of BrO in the extra-tropical lowermost stratosphere, obtained
450 on RF15 by the CIMS and DOAS instruments.

451 **4.3 Ozone over the TWP warm pool**

452 The CONTRAST research flights included significant profile measurements spanning from near
453 the surface to above 14 km. Together with takeoffs and landings there were nearly 100 vertical
454 profiles over the domain. CONTRAST has provided the first extensive in situ measurements of
455 ozone within the UT over the warm pool of the TWP, where routine sampling does not occur and
456 very few prior observations (e.g., Rex et al., 2014 and references therein) are available. Ozone
457 profiles typical of the CONTRAST measurements, from RF04, are shown in Figure 10a. Ozone
458 in the UT (> 9 km) was near 20 ppbv throughout the experiment, with little variability either in
459 space or time (Figure 11). Ozone mixing ratios near the surface and in the MBL were typically

between 10 and 20 ppbv, as shown in Figure 10a for RF04, as well as throughout other CONTRAST flights (Figure 11). Consequently, the persistent upper tropospheric ozone values near 20 ppbv are consistent with the strong influence of convective outflow of low-level air (Pan et al., 2015).

The airborne measurements during CONTRAST often showed enhanced ozone over the lower-middle troposphere (~3-9 km), with values typically 40-80 ppbv (Figure 10a). The enhanced ozone occurred in persistent layers and filaments, which were furthermore characterized by extremely dry air (relative humidity < 45%) (Figure 10b). The strong correlation of enhanced ozone with dry layers is similar to previous observations (e.g. Thouret et al., 2001; Hayashi et al., 2008), although the layers observed in CONTRAST were more persistent. These dry, enhanced ozone layers over ~3-9 km (320-340 K in potential temperature coordinates) were a ubiquitous feature observed during CONTRAST. The layers occurred so frequently that the statistical distribution of ozone over this altitude region exhibits a bi-modal distribution, with a primary mode near 20 ppbv and an enhanced mode centered on ozone near 60 ppbv (Pan et al., 2015).

The mechanisms producing the structure shown in Figure 10 are a topic of active research. Contributions from large-scale dynamics, i.e. transport and mixing, as well as ozone production in plumes of biomass burning (Anderson et al., 2016) are leading candidates under investigation. Figure 11 shows that the occurrence of the ozone layers are mainly in the ~320-340 K isentropic levels. At these levels isentropic mixing could connect the air mass in the tropical low to mid-troposphere to the UTLS region in midlatitudes near the subtropical jet. This structure suggests a large-scale dynamical influence, which is consistent with the interpretations of the dry layers by the TOGA COARE community (e.g., Yoneyama and Parsons, 1999). On the other hand, tracer measurements show a significant signature of combustion of plant matter that provides

compelling chemical evidence that biomass burning also contributes significantly to the enhanced O_3 layers (Anderson et al., 2016). Because the dataset includes a large suite of chemical species that can provide chemical signatures of transport and chemical processing, CONTRAST data can be used to better quantify the contributing mechanisms of these high ozone – low water structures.

4.4 Pollution in the tropics and at the TTL level

Anthropogenic impact on the remote TWP region was the main focus of several previous experiments (Gregory et al., 1999; Kondo et al., 2002; Jacob et al., 2003). Although not explicitly included in the original objectives of the CONTRAST experiment, the influence of human activity on the chemical composition of the remote TWP warm pool region is directly relevant to ozone budget, oxidizing capacity, and impact of convection for this region of the atmosphere. CONTRAST data have provided the first intensive chemical sampling of the troposphere overlying the TWP warm pool during NH winter. During the experiment, GV flights targeted a number of cases where a significant difference of polluted versus clean air masses was observed. These cases include: 1) measurements both north and south of a well-defined ITCZ (RF10), 2) measurements in front of and behind a shear line, which moved into tropics from the northeast Asian continent (RF06), 3) sampling of a pollution plume brought into the TWP domain by the jet stream and the region's anticyclonic flow (RF10, the "CO river"), and 4) observations of the polluted TTL over Papua New Guinea versus the more pristine TTL over the Coral Sea (RF14).

Figure 12 shows the successful sampling of the long-range transport of air pollution on 10 February 2014 (RF10). Based on the chemical forecast by NCAR CAM-chem-SD (see figure 6) and MACC CO field (not shown), the flight was designed to target a pollution plume that was flowing into the Guam domain from Southeast Asia and along the equator flank of the jetstream. The flight succeeded in documenting the highest mixing ratio of CO measured over the TWP in the entire campaign (~130 ppbv), providing an interesting case characterized as the "CO river". The figure also shows a layer of high ozone well correlated with elevated CO, indicating the associated photochemical production of O_3 from pollutants emitted over the continent. Additional hydrocarbon measurements by TOGA suggest biomass burning may have played a role in the origin of this plume.

The TTL survey flight on 22 February 2014 (RF14) observed stark differences between strongly polluted and clean regions of the TTL. This 9 hour and 30 min flight covered a large latitude range, from Guam to the Coral Sea (13.5°N – 20°S) (Figure 13a). The flight provided the southernmost set of observations for the entire campaign. Most of the flight was downwind from active convection. While under convective influence, the TTL was moderately polluted for most of the flight, as shown by elevated levels of benzene (Figure 13b). The highest level of pollution was observed over the island of Papua New Guinea (PNG) (~8°S), where the GV flew through moderate deep convection and sampled the influence of direct convective pumping of biomass burning on the island. A region of extremely clean air was sampled over the Coral Sea (~18°S), indicated by the mixing ratio of benzene being near the detection limit of the TOGA instrument. This clean air region provided unique measurements to chemically characterize the pristine tropical UT

527 conditions with no immediate pollution source and under calm weather. The contrast of
528 clean versus polluted air in the TTL is important for characterizing the impact of
529 anthropogenic activity, coupled with deep convection around the maritime continents, on
530 the composition of the UT.

531 **4.5 GV–ozonesonde coordinated flights**

532 A significant fraction of prior ozone profile measurements in the tropical troposphere have
533 been obtained by ozonesondes. These measurements include data from the Southern
534 Hemisphere ADditional OZonesondes (SHADOZ) network (Thompson et al., 2011), which
535 does not routinely sample the warm pool atmosphere over the TWP (Figure 1 shows
536 ozonesonde launch locations), as well as ozonesondes launched from several ship- based
537 field experiments in the TWP (Rex et al., 2014, and references therein). Extremely low
538 ozone values at the level of convective outflow in UT (i.e., at the base of the TTL) have been
539 reported from these ozonesonde measurements in the TWP (Kley et al., 1996; Rex et al.,
540 2014). The low ozone environment has been hypothesized to suppress the presence of
541 hydroxyl radicals (OH), which controls the lifetime of a large suite of chemical species (Rex
542 et al., 2014). However, the physical interpretation of these low ozone cases is challenged
543 by the uncertainty in background current calibration of ozonesondes (Vömel and Diaz,
544 2010).

545 Quantification of O_3 at the level of convective outflow in the UT over the TWP, and
546 assessment of ozonesonde calibration, were motivating factors for the planning of a GV
547 overflight of Manus Island (2° S) within a short window of an ozonesonde launch by the
548 CAST team. Overflights of Manus by the GV were carried out on 4 and 22 of February 2014

549 (RF09 and RF14). Flight permission issues and air traffic control challenges posed
550 significant limitations to the flights and prevented the GV from performing a complete
551 profile near the site of the ozonesonde launch. Specifically, RF09 was the first flight
552 operation crossing the equator into the Port Moresby FIR working with Papua New Guinea
553 (PNG) ATC. The flight plan started with MBL sampling first once entered Port Moresby FIR,
554 followed by ascending to the flight ceiling near the Manus Island. When GV arrived on
555 station near the Manus Island for collocated profiling with the ozonesonde launch, the PNG
556 ATC kept the plane at flight level 34 Kft for a commercial flight to pass at 38 Kft. This
557 altitude hold used up the filed flight pattern, which was planned to loop up to the TTL level.
558 The ATC did not give the team a chance to repeat the flight pattern at higher altitudes once
559 the commercial airliner passed. The lessons learned from RF09 led to a different strategy
560 in planning for RF14, resulting in a successful partial profile at the TTL level with the co-
561 located ozonesonde from Manus Island in this second attempt. Despite the difficulties in
562 operations, the two flights obtained co-located partial profiles of O_3 that have been used to
563 validate the ozonesonde calibration (Newton et al., 2016).

564

565 Figure 14 shows the flight track, ozonesonde profile, and the co-located GV partial O_3
566 profile between 13 and 15 km during RF14. The GV data were obtained for the altitude
567 range where the question of whether near-zero ozone in the balloon observations is
568 actually real (Kley et al., 1996) or is due to varying background current (Vömel and Diaz,
569 2010) had yet to be resolved. The GV in situ O_3 instrument, based on chemiluminescence
570 (Ridley et al., 1992), has a low detection limit of 0.1 ppbv and high vertical resolution of

571 near 7 m during profiling. For the entire campaign, the lowest measured amount of ozone
572 in the upper troposphere was 13 ppbv.

573 The intercomparison results show a consistent picture. By not exposing the ozonesonde to
574 ozone during preparation, and by assuming a constant background current measured in
575 the laboratory immediately before launch, ozonesonde profiles were measured and agreed
576 with the GV to 3 ppbv between 150 and 200 mb (Newton et al, 2016). This is within the
577 expected error limits of the sondes. Further, during the entire CAST ozonesonde campaign
578 the minimum repeatable ozone concentration in the TTL from the Manus ozonesondes was
579 12 ppbv, again very consistent with the GV.

580

581 **5. Forward from the field phase**

582 The CONTRAST experiment succeeded in obtaining a large suite of trace gas measurements,
583 together with dynamical and microphysical variables, under a wide range of conditions
584 over the TWP. The intensive sampling of actinic flux, ozone, water vapor, and other active
585 species will allow constrained photochemical calculation of hydroxyl radical over the TWP,
586 which will lead to a better understanding of the processes that control atmospheric
587 oxidation capacity in the tropical western Pacific. Oxidation processes in the tropical
588 atmosphere play a major role in the global budget of many trace gases, including
589 greenhouse gases. The region has added significance because the major transport of
590 tropospheric air into the lower stratosphere occurs over the TWP.
591 The flights successfully sampled air masses in convective updraft, and outflow both near
592 and downstream of active convection. The data will enable individual case studies and

593 statistical quantification of the impact of convection and convective transport on the
594 vertical distribution of a wide range of compounds with different photochemical lifetimes.
595
596 Within the context of the coordinated experiments, the CONTRAST, ATTREX, and CAST
597 campaigns obtained the vertical distribution of a large number of reactive gases relevant to
598 chemistry-climate interactions, especially a unique data set of halogenated VSL species
599 from the oceanic surface to the LS over the TWP. These measurements, along with
600 measurements of inorganic halogen product gases, will add new capability to evaluate the
601 processes that control the reactive halogen chemistry, extending from the MBL, through
602 the TTL, and into the LS. The ocean sources and sinks of these gases, as well as a range of
603 oxygenated organic gases (such as formaldehyde) will be examined from the
604 measurements that were collected during the campaigns. Accurate representation of the
605 impact of deep convection on the chemical environment is a major challenge for CCMs.
606 Observational information from CONTRAST will provide important constraints, especially
607 for the remote TWP troposphere.
608
609 Finally, CONTRAST data provided the first intensive in situ observations of ozone in the
610 TTL over the oceanic warm pool. The measurements filled an important data gap by
611 coordinating in situ measurements with co-located ozonesonde profiles, which resulted in
612 a new understanding of ozonesonde uncertainty (Newton et al., 2016) and quantified the
613 low ozone level over the TWP TTL. The repeated vertical profiles of chemical distributions
614 during CONTRAST also led to the discovery of a bimodal ozone distribution in the free
615 troposphere between ~ 3-9 km over the TWP (Pan et al., 2015). The controlling

616 mechanism(s) of the two modes, and how well the modes are represented in global CCMs,
617 are topics of active research (Anderson et al., 2016).

618 CONTRAST data are publicly available for all researchers and can be obtained at
619 http://data.eol.ucar.edu/master_list/?project=CONTRAST.

620

621

622 **Acknowledgements**

623 Funding for this work was provided by the National Science Foundation (NSF) via its
624 sponsorship of the National Center for Atmospheric Research (NCAR).

625 The CONTRAST experiment was sponsored by the (NSF). We acknowledge the excellent
626 field project support provided by NCAR/EOL during flight operations. We give special
627 thanks to the GV pilots and mission coordinators for their knowledge, skills and dedication;
628 these were essential to the success of this campaign.
629 The MACC forecasts was funded by the European Union's Seventh Framework Programme
630 (FP7) under grant agreement no. 283576.

631 The views, opinions, and findings contained in this report are those of the author(s) and
632 should not be construed as an official National Oceanic and Atmospheric Administration or
633 U.S. Government position, policy, or decision.

634

635 **Appendix A. List of Abbreviations**

636 ATTREX: Airborne Tropical Tropopause Experiment

637 BIBLE: Biomass Burning and Lightning Experiment

638 CAM-chem: Community Atmosphere Model with Chemistry

639 CAST: Coordinated Airborne Studies in the Tropics

640 CCM: Chemistry Climate Model

641 CONTRAST: Convective Transport of Active Species in the Tropics

642 ECMWF: European Center for Medium-Range Weather Forecasting

643 ENSO: El Niño-Southern Oscillation

644 EOL: Earth Observing Laboratory

645 FAAM: Facility for Airborne Atmospheric Measurements

646 FIR: Flight Information Region

647 GEOS-5: Goddard Earth Observing System Model, Version 5

648 GFS: Global Forecast System

649 GMAO: Global Modeling and Assimilation Office

650 GTE: Global Tropospheric Experiment

651 HIAPER: High-performance Instrumented Airborne Platform for Environmental Research

652 IGAC: International Global Atmospheric Chemistry

653 ITCZ: Inter Tropical Convergence Zone

654 MACC: Monitoring Atmospheric Composition and Climate

655 MJO: Madden-Julian Oscillation

MTSAT: Multi-functional Transport Satellite

RAQMS: Real-time Air Quality Modeling System

SHADOZ: Southern Hemisphere Additional Ozonesondes

SPARC: Stratospheric Processes and their Role in Climate

TOGA COARE: Tropical Ocean – Global Atmosphere (TOGA) Coupled Ocean Atmosphere Response Experiment (COARE)

TORERO: Tropical Ocean tRoposphere Exchange of Reactive halogens and Oxygenated hydrocarbons

WCRP: World Climate Research Programme

WOUDC: World Ozone and Ultraviolet Radiation Data Centre

WRF: Weather Research and Forecasting Model

672 **References**

673 Anderson, D. C., et al., 2016: A pervasive role for biomass burning in tropical high
674 ozone/low water structures, Nature Communications, 7, doi:10.1038/ncomms10267.

675 Andrews, S. J. et al., A comparison of very short-lived halocarbon (VSLS) aircraft
676 measurements in the West Tropical Pacific from CAST, ATTREX and CONTRAST,
677 submitted to ACPD, 2015.

678 Apel, E. C., Hornbrook, R. S., Hills, A. J, Blake, N. J., Barth, M., Crawford, J. H., Homeyer, C. R.,
679 Cantrell, C. A., Rutledge, S., Weinheimer, A. J., Fried, A., Blake, D. R., Brune, W., Pollack, I.,
680 Peischl, J, Ryerson, T., and Riemer, D. D, 2015: Upper tropospheric ozone production
681 from lightning NOx-impacted convection: Smoke ingestion case study from the DC3
682 campaign, J. Geophys. Res. Atmos., 120, doi:10.1002/2014JD022121.

683 Baidar, S., H. Oetjen, S. Coburn, B. Dix, I. Ortega, R. Sinreich, and R. Volkamer, 2013: The CU
684 Airborne MAX-DOAS Instrument: Vertical Profiling of Aerosol Extinction and Trace
685 Gases. Atmos. Meas. Tech., 6(3), 719-719-739, doi: 10.5194/amt-6-719-2013.

686 Bergman, J. W., E. J. Jensen, L. Pfister, Q. Yang, 2012: Seasonal differences of vertical-
687 transport efficiency in the tropical tropopause layer: on the interplay between tropical
688 deep convection, large-scale vertical ascent, and horizontal circulations, J. Geophys. Res.,
689 117, D05302, doi: 10.1029/2011JD016992.

690 Calvert, J., A. Mellouki, and J. Orlando, 2011: Mechanisms of Atmospheric Oxidation of the
691 Oxygenates, Oxford University Press, USA, 1634 pp.

692 Carpenter, L. J. and S. Reimann (Lead Authors), J.B. Burkholder, C. Clerbaux, B.D. Hall, R.
693 Hossaini, J.C. Laube,and S.A. Yvon-Lewis, 2014: Ozone-Depleting Substances (ODSs) and
694 Other Gases of Interest to the Montreal Protocol, Chapter 1 in Scientific Assessment of
695 Ozone Depletion: 2014, Global Ozone Research and Monitoring Project –Report No. 55,
696 World Meteorological Organization, Geneva, Switzerland.

697 Carpenter, L. J., et al., 2010: Seasonal characteristics of tropical marine boundary layer air
698 measured at the Cape Verde Atmospheric Observatory, J. Atmos. Chem. 67, 87-140,
699 doi:10.1007/s10874-011-9206-1.

700 Carpenter, L. J., MacDonald, S. M., Shaw, M. D., Kumar, R., Saunders, R. W., Parthipan, R.,
701 Wilson, J., and Plane, J. M. C., 2013: Atmospheric iodine levels influenced by sea surface
702 emissions of inorganic iodine, Nature Geosci., 6, 108–111, doi:10.1038/ngeo1687.
703 Corti, T., B. P. Luo, T. Peter, H. Vo¨mel, and Q. Fu (2005), Mean radiative energy balance and
704 vertical mass fluxes in the equatorial upper troposphere and lower stratosphere,
705 Geophys. Res. Lett., 32, L06802, doi:10.1029/2004GL021889.

706 Crawford, J. H., and Coauthors, 1997: Implications of large scale shifts in tropospheric NOx
707 levels in the remote tropical Pacific, J. Geophys. Res., 102(D23), 28447–28468,
708 doi:10.1029/97JD00011.

709 Dima, I. M., and J. M. Wallace, 2007: Structure of annual-mean equatorial planetary waves. J.
710 Atmos. Sci., 64, pp. 2862-2880.

711 Dix, B., S. Baidar, J.F. Bresch, S.R. Hall, K.S. Schmidt, S. Wang, and R. Volkamer. Detection of
712 Iodine Monoxide in the Tropical Free Troposphere. 2013, PNAS, 110(6), 2035-2040,
713 doi: 10.1073/pnas.1212386110.

714 Fernandez, R. P., R. J. Salawitch, D. E. Kinnison, J.-F. Lamarque, and A. Saiz-Lopez, 2014:
715 Bromine partitioning in the tropical tropopause layer: implications for stratospheric
716 injection, Atmos. Chem. Phys., 14, 17857-17905, doi: 10.5194/acp-14-13391-2014.

717 Flemming, J., A. Inness, H. Flentje, V. Huijnen, P. Moinat, M. G. Schultz, and O. Stein, 2009:
718 Coupling global chemistry transport models to ECMWF's integrated forecast system,
719 Geosci. Model Dev., 2, 253-265, doi: 10.5194/gmd-2-253-2009.

720 Frieler, K., M. Rex, M., R. J. Salawitch, T. Canty, M. Streibel, R. M. Stimpfle, K. Pfeilsticker, M.
721 Dorf, D. K. Weisenstein, and S. Godin-Beekmann, S., 2016: Toward a better quantitative
722 understanding of polar stratospheric ozone loss. Geophys. Res. Lett, 33,
723 10.1029/2005GL025466.

724 Fueglistaler, S., H. Wernli, and T. Peter, 2004: Tropical troposphere-to-stratosphere
725 transport inferred from trajectory calculations, J. Geophys. Res., 109, D03108, doi:
726 10.1029/2003JD004069.

727 Fueglistaler, S., A. E. Dessler, T. J. Dunkerton, I. Folkins, Q. Fu, and P. W. Mote, 2009: Tropical
728 Tropopause Layer, Rev. Geophys., 47, RG1004, doi: 10.1029/2008RG000267.

729 Gregory, G. L., et al. (1999), Chemical characteristics of Pacific tropospheric air in the region
730 of the Intertropical Convergence Zone and South Pacific Convergence Zone, J. Geophys.

Res., 104(D5), 5677–5696, doi:10.1029/98JD01357.Hoell, J. M., and Coauthors, 1999: Pacific Exploratory Mission in the tropical Pacific: PEM-Tropics A, August-September 1996, J. Geophys. Res., 104(D5), 5567–5583, doi: 10.1029/1998JD100074.

Hayashi, H., Kita, K., and Taguchi, S.: Ozone-enhanced layers in the troposphere over the equatorial Pacific Ocean and the influence of transport of midlatitude UT/LS air, Atmos. Chem. Phys., 8, 2609-2621, doi:10.5194/acp-8-2609-2008, 2008.

Holton, J.R., and A. Gettelman, 2001: Horizontal transport and the dehydration of the stratosphere, Geophys. Res. Let., 28, 14, 2799-2802, doi:10.1029/2001GL013148.

Huey, L. G. (2007), Measurement of trace atmospheric species by chemical ionization mass spectrometry: Speciation of reactive nitrogen and future directions, Mass Spectrom. Rev., 26(2),166-184.

Jacob, D.J., J.H. Crawford, M.M. Kleb, V.S. Connors, R.J. Bendura, J.L. Raper, G.W. Sachse, J.C. Gille, L. Emmons, and C.L. Heald, The Transport and Chemical Evolution over the Pacific (TRACE-P) aircraft mission: design, execution, and first results, J. Geophys. Res., 108, 9000, 10.1029/2002JD003276, 2003.

Jensen, E. J. and Coauthors, The NASA Airborne Tropical TRopopause EXperiment (ATTREX): high-altitude aircraft measurements in the tropical western Pacific, submitted to Bull. Amer. Meteor. Soc.

749 Kley, D., P. J. Crutzen, H. G. J. Smit, H. Vömel, S. J. Oltmans, H. Grassl, V. Ramanathan, 1996:
750 Observations of near-zero ozone concentrations over the convective Pacific: effects on
751 air chemistry, Science, 274, 230-233, doi:10.1126/science.274.5285.230.

752 Ko, M. K. W., N.-D. Sze, C. J. Scott, and D. K. Weisenstein (1997), On the relation between
753 stratospheric chlorine/bromine loading and short-lived tropospheric source gases, J.
754 Geophys. Res., 102(D21), 25507–25517, doi:10.1029/97JD02431.

755 Kondo, Y., and Coauthors, 2002: Effects of biomass burning, lightning, and convection on O3,
756 CO, and NOy over the tropical Pacific and Australia in August–October 1998 and 1999, J.
757 Geophys. Res.,107, 8402, doi: 10.1029/2001JD000820.

758 Krüger, K., S. Tegtmeier, and M. Rex, 2008: Long-term climatology of air mass transport
759 through the Tropical Tropopause Layer (TTL) during NH winter, Atmos. Chem. Phys., 8,
760 813–823, doi:10.5194/acp-8-813-2008.

761 Langner, J and H. Rodhe, 1991: A global three-dimensional model of the tropospheric sulfur
762 cycle, J. Atmos Chem. 13, 225-264.

763 Lamarque, J.-F., and Coauthors, 2012: CAM-chem: description and evaluation of interactive
764 atmospheric chemistry in the Community Earth System Model, Geosci. Model Dev., 5,
765 369-411, doi:10.5194/gmd-5-369-2012.

766 Liu, C., and E. J. Zipser, 2015: The global distribution of largest, deepest, and most intense
767 precipitation systems, Geophys. Res. Lett., 42, 3591-3595, doi:10.1002/2015GL063776.

768 Millet, D. B., Guenther, A., Siegel, D. A., Nelson, N. B., Singh, H. B., de Gouw, J. A., Warneke, C.,
769 Williams, J., Eerdekens, G., Sinha, V., Karl, T., Flocke, F., Apel, E., Riemer, D. D.,
770 Palmer, P. I., and Barkley, M.: Global atmospheric budget of acetaldehyde: 3-D model
771 analysis and constraints from in-situ and satellite observations, Atmos. Chem. Phys., 10,
772 3405-3425, doi:10.5194/acp-10-3405-2010, 2010.

773 Newell, R. E., and S. Gould-Stewart, 1981: A stratospheric fountain?, J. Atmos. Sci., 38, 2789-
774 2796, doi: 10.1175/1520-0469(1981)038<2789:ASF>2.0.CO;2.

775 Newton, R., Vaughan, G., Ricketts, H. M. A., Pan, L. L., Weinheimer, A. J., and Chemel, C. 2016:
776 Ozonesonde profiles from the West Pacific Warm Pool: measurements and validation,
777 Atmos. Chem. Phys., 16, 619-634, doi:10.5194/acp-16-619-2016.

778 Pan, L. L., and L. A. Munchak, 2011: Relationship of cloud top to the tropopause and jet
779 structure from CALIPSO data, J. Geophys. Res., 116, D12201,
780 doi:10.1029/2010JD015462.

781 Pan, L.L., S. B. Honomichl, W. J. Randel, E. C. Apel, E. L. Atlas, S. P. Beaton, J. F. Bresch, R.
782 Hornbrook, D. E. Kinnison, J-F Lamarque, A. Saiz-Lopez, R. J. Salawitch, and A. J.
783 Weinheimer, 2015: Bimodal distribution of free tropospheric ozone over the tropical
784 western Pacific revealed by airborne observations, Geophys. Res. Lett., Doi:
785 10.1002/2015GL065562.

786 Pierce, R. B., and Coauthors, 2007: Chemical data assimilation estimates of continental U.S.
787 ozone and nitrogen budgets during the Intercontinental Chemical Transport
788 Experiment–North America, J. Geophys. Res., 112, D12S21, doi:10.1029/2006JD007722.

789 Randel, W. J., E. J. Jensen, 2013: Physical processes in the tropical tropopause layer and
790 their roles in a changing climate, Nature Geoscience, 6, doi:10.1038/NGEO1733.

791 Rex, M., and Coauthors, 2014: A tropical West Pacific OH minimum and implications for
792 stratospheric composition, Atmos. Chem. Phys., 14, 4827-4841, doi:10.5194/acp-14-
793 4827-2014.

794 Ridley, B. A., F. E. Grahek, and J. G. Walega, A small, high-sensitivity, medium-response
795 ozone detector for measurements from light aircraft, J. Atmos. Oceanic Technol., 9, 142-
796 148, 1992.

797 Saiz-Lopez A., and Coauthors, 2012: Estimating the climate significance of halogen-driven
798 ozone loss in the tropical marine troposphere, Atmos. Chem. Phys., 11, 32003-32029,
799 doi:10.5194/acp-12-3939-2012.

800 Saiz-Lopez, A., and R. von Glasow, 2012: Reactive halogen chemistry in the troposphere,
801 Chem. Soc. Rev., 41, 6448-6472, doi:10.1039/C2CS35208G.
802 Saiz-Lopez, A., R. P. Fernandez, C. Ordóñez, D. E. Kinnison, J. C. Gómez Martín, J. F. Lamarque,
803 and S. Tilmes, 2014: Iodine chemistry in the troposphere and its effect on ozone, Atmos.
804 Chem. Phys., 14(23), 13,119–13,143.
805 Saiz-Lopez, A., et al. , 2015: Injection of iodine to the stratosphere, Geophys. Res. Lett., 42,
806 6852–6859, doi:10.1002/2015GL064796.
807 Salawitch, R. J., D. K. Weisenstein, L. J. Kovalenko, C. E. Sioris, P. O. Wennberg, K. Chance, M.
808 K. W., Ko, and C. A. McLinden, 2005: Sensitivity of ozone to bromine in the lower
809 stratosphere, Geophys. Res. Let., 32, L05811, doi: 10.1029/2004GL021504.

Schoeberl, M. R. and A. E. Dessler, 2011: Dehydration of the stratosphere, Atmos. Chem. Phys., 11, 8433-8446, doi:10.5194/acp-11-8433-2011, 2011.

Skamarock, W. C., and Coauthors, 2008: A Description of the Advanced Research WRF Version 3, NCAR Technical Note NCAR/TN-475+STR, doi: 10.5065/D68S4MVH.

Stephens, G. L., et al., 2008: CloudSat mission: Performance and early science after the first year of operation, J. Geophys. Res., 113, D00A18, doi:10.1029/2008JD009982.

Takahashi, H., and Z. Luo, 2012: Where is the level of neutral buoyancy for deep convection?, Geophys. Res. Lett., 39, L15809, doi:10.1029/2012GL052638.

Thompson A. M., S. J. Oltmans, D. W. Tarasick, P. von der Gathen, H. , (2011) Strategic Ozone Sounding Networks: Review of Design and Accomplishments, Atmospheric Environment, 45, 13, 2145-2163, doi:10.1016/j.atmosenv.2010.05.002.

Thouret, V., J. Y. N. Cho, M. J. Evans, R. E. Newell, M. A. Avery, J. D. W. Barrick, G. W. Sachse, and G. L. Gregory (2001), Tropospheric ozone layers observed during PEM-Tropics B, J. Geophys. Res., 106(D23), 32527–32538, doi:10.1029/2001JD900011.

Vömel, H and K. Diaz (2010), Ozone sonde cell current measurements and implications for observations of near-zero ozone concentrations in the tropical upper troposphere, Atmos. Meas. Tech., 3, 495-505.

Volkamer, R., Baidar, S., Campos, T.L., Coburn, S., DiGangi, J.P., Dix, B., Eloranta, E.W., Koenig, T.K., Moley, B., Ortega, I., Pierce, B.R., Reeves, M., Sinreich, R., Wang, S-Y., Zondlo, M.A. and Romashkin, P.A., 2015: Aircraft measurements of BrO, IO, glyoxal, NO2, H2O, O2-O2 and aerosol extinction profiles in the tropics: Comparison with aircraft-/ship-based in situ and lidar measurements, Atmos. Meas. Tech. 8, 2121-2148. doi:10.5194/amt-8-2121-2015.

833 Wang, S-Y., J.A. Schmidtd, S. Baidar, S. Coburn, B. Dix, T.K. Koenig, E.C. Apel, D. Bowdalo, T.L.
834 Campos, E. Eloranta, M.J. Evans, J.P. diGangii, M.A. Zondlo, R-S. Gao, J.A. Haggerty, S.R.
835 Hall, R.S. Hornbrook, D.J. Jacob, B. Morley, B.R. Pierce, M. Reeves, P.A. Romashkin, A. ter
836 Schure, and R. Volkamer, 2015: Active and Widespread Halogen Chemistry in the
837 Tropical and Subtropical Free Troposphere, Proc. Natl. Acad. Sci., 112 (30), 9281–9286.
838 doi: 10.1073/pnas.1505142112.
839 Webster, P. J. and R. Lukas, 1992: TOGA COARE: The Coupled Ocean-Atmosphere Response
840 Experiment, Bull. Amer. Meteor. Soc., 73, 1377-1416, doi: 10.1175/1520-
841 0477(1992)073<1377:TCTCOR>2.0.CO;2.
842 Wyrtki, K., 1989: Some thoughts about the West Pacific Warm Pool, in: J. Picaut, et al. Eds.,
843 Proc. of Western Pacific International Meeting and Workshop on TOGA COARE. 99-109.
844 Yang, Q., Q. Fu, and Y. Hu (2010), Radiative impacts of clouds in the tropical tropopause
845 layer, J. Geophys. Res., 115, D00H12, doi:10.1029/2009JD01239.
846 Yoneyama, K., and D. B. Parsons, 1999: A mechanism for the intrusion of dry air into the
847 tropical western Pacific region. J. Atmos. Sci., 56, 1524–1546.
848
849

Figure Captions

Figure 1. Thirty-year climatology of January-February sea surface temperature (SST), highlighting the TWP warm pool. The SST, shown by the color shaded contours, is from NOAA Optimum Interpolation data version 2 (Reynolds et al., 2002). The 30-year mean 193 K temperature contour at the 100 hPa pressure level (black contour) is shown to indicate the coldest region of TTL. Also shown are locations of ozonesonde measurements (white circles) obtained from WOUDC (http://woudc.org/home.php), which include the SHADOZ stations.

Figure 2. Concept of the coordinated campaigns. This schematic highlights the three research aircraft and the altitude ranges of their sampling in relation to the dynamical background. The key feature of the background is deep convection that nearly reaches the tropopause and which pumps marine boundary layer air into the TTL (~13-17 km). The level of full-sky net zero radiative heating, estimated to be near 14 km, is typically used to indicate the transition into mean upward motion driven by large-scale dynamical control (Corti et al., 2005).

Figure 3. Some key UTLS dynamical elements of the TWP during the CONTRAST campaign period. The figure shows the campaign domain, centered at Guam. The magenta and cyan circles indicate the nominal GV flight range (1000 and 1500 nmi radius respectively). The gray-blue-yellow-orange shading shows the 12-14 km cloud fractions calculated using the CloudSat data, indicating the region dominated by frequent deep convection. The pink stipple shading shows the frequency of 200 hPa PV>1 PVU (1 PVU = 10^{-6} m^{-2} K s^{-1} kg^{-1}) during the campaign period, based on the GFS analyses. The increase in this frequency of

PV>1 PVU indicates the transition from the tropics to extratropics. The red contours are selected 200 hPa geopotential height (GPH, in km) levels indicating the region under the influence of mean anticyclonic circulation (Dima and Wallace, 2007). Blue arrows show the 200 hPa wind field; the 50 and 60 m/s wind speed contours are used to indicate the seasonal mean location of the northern hemispheric subtropical jet.

Figure 4. CONTRAST GV payload configuration. See Table 1 for instrument details. The cabin instruments are shown by their inlet locations (with exception of TOGA, its inlet was behind the fuselage in this takeoff photo). The colors are used to indicate the instrument type: chemistry (red), microphysics (purple), radiation (magenta), and the digital camera (green).

Figure 5. CONTRAST flight operation domain and the GV flight tracks (RF02-RF16). The operational domain is marked by the magenta and cyan circles, which indicate the nominal GV flight range with or without extensive profiling (1000 and 1500 nmi radius respectively). The red ring close to Guam indicates the region covered by the Guam ATC radar. The green lines mark the boundaries of Flight Information Regions (FIRs). As shown, most of the GV flights were operated within the Oakland Oceanic FIR (USA). Three additional FIRs flown were Fukuoka (JPN), Port Moresby (PNG), and Brisbane (AUS).

Figure 6. Examples of operational weather and chemical forecast plots for RF10 (flight day 8 February 2014). a) CAM-chem-SD 200 hPa CO (color shade) and wind field (pink arrows) forecast that shows an intense CO plume moving into the Guam domain following the jet stream. Also shown is the 2 PVU contour at 200 hPa, which marks the division of tropical UT and extratropical LS. b) The WRF forecast of surface wind (wind barb vectors) and

894 precipitating convection (shaded), which predicts an ITCZ near 7°N indicated by the
895 surface wind convergence and the line of convection.

896 **Figure 7.** An example of a coordinated flight and the GV targeting active convection. This
897 figure shows the real-time display from the Catalog Map on 13 Feb 2014 near 0400 UTC,
898 around the time the GV sampled the region of convective outflow (see Figure 8). Active
899 convection was widespread southwest of Guam, as revealed by the MTSAT IR (color
900 shading) and visible (gray) channels. The yellow and red lines show flight tracks for each of
901 the three aircraft (red indicates the track for the last hour).

902 **Figure 8.** Time series of flight altitudes, vertical velocity, and mixing ratios of selected
903 short-lived compounds during a 3-hour segment of RF11 (12 February 2014) when the GV
904 was targeting the outflow from active convection (see GV location and the region of active
905 convection during this time period in Fig. 7). The active convection regions are indicated by
906 increases in updraft velocity (~ 5 m/s and 13 m/s, respectively). For the aircraft location
907 and the convection, see Fig. 7, which shows satellite IR channel near 04:00 UTC. As
908 indicated by the track in Fig. 7, the GV repeatedly targeted the convective region at
909 different altitudes. The two time periods of successful sampling of fresh outflow
910 (associated with the updraft velocity 5 m/s and 13 m/s) the GV was at 43 Kft (~ 14 km)
911 and 40 Kft (~11 km), respectively. The location of the updraft was in the vicinity of the
912 aircraft position shown in Fig. 7. The tropopause was at ~17 km. The corresponding
913 enhancements of short-lived species in the UT are shown using TOGA observations of
914 acetaldehyde (CH_3CHO), methyl ethyl ketone (MEK; $CH_3C(O)CH_2CH_3$), and dimethyl sulfide
915 (DMS; CH_3SCH_3). DMS and MEK are below the detection limit (1 pptv) for the majority of

916 the UT time segment with the exception of the updraft region, especially during 03:49 -
917 03:54 UTC.

918 **Figure 9**. (a) Vertical distribution of the total bromine content from two short-lived
919 organic bromocarbons (2x CH_2Br_2 + 3x$CHBr_3$) from GV TOGA (gray) and whole air
920 samplers on all three aircraft (Cyan: BAe146, Blue: GV, Red: Global Hawk). The gray line
921 represents the median profile derived using all four data sets. (b) Latitude-height cross-
922 section of the mean cloud fraction of the region (140° and 150° E) during the period of the
923 CONTRAST campaign, calculated using CloudSat satellite data.

924 **Figure 10.** Ozone (a) and water vapor (b) data from RF04, as an example of the ozone
925 profile structure, with layers of ozone enhancement that are coincident with layers of
926 water vapor reduction. Relative humidity (RH) levels corresponding to the measured
927 water vapor and temperature are also shown (black curves).
928

929 **Figure 11.** The GV flight tracks for all flights colored by the O_3 mixing ratio. Also included
930 are mean large-scale dynamical structures of the campaign period and domain,
931 represented by the tropopause height (black dots), 2 PVU contour (red dash), subtropical
932 jet location (40, 50, 60 m/s horizontal wind, blue contour) and mean isentropes, all given in
933 sectional zonal mean for 130°-160° E longitude range.
934

935 **Figure 12.** (a) CAM-chem-SD model simulation of CO at the 300 hPa level as well as the
936 aircraft flight track (yellow) and (b) the GV measurements of CO and O_3 in the "CO river"
937 during RF10 on 8 February 2014. The portion of the flight track corresponding to the in

situ profile shown in (b) is marked in red on the map (a). The maximum CO enhancement is shown to be ~ 8.5 km altitude (~ 300hPa pressure level).

Figure 13. Chemical gradients at the TTL level shown by TOGA Benzene data from RF14 flight on 22 February 2014. (a) The flight track shows the large latitude range (~15 ° N – 20°S) sampled. The flight was conducted in three FIRs: 1) Oakland Oceanic (USA), 2) Port Moresby (PNG) and 3) Brisbane (AUS). (b) Benzene mixing ratio from TOGA highlights the strong contrast of air over PNG (~8°S) and the Coral Sea (south of 10°S). The black arrows above the tracks indicate the outbound/inbound flight directions.

Figure 14. (a) GV-ozonesonde coordinated flight during RF14, 22 February 2014 with Manus Island ozonesonde launch. GV flight track is shown in orange on the map. (b) GV in situ ozone, sampled during a dip from west of Manus Island from 45 Kft to 41 Kft, is shown in magenta, while ozonesonde measurements of ozone (black), temperature (red) and potential temperature (green) are also shown.

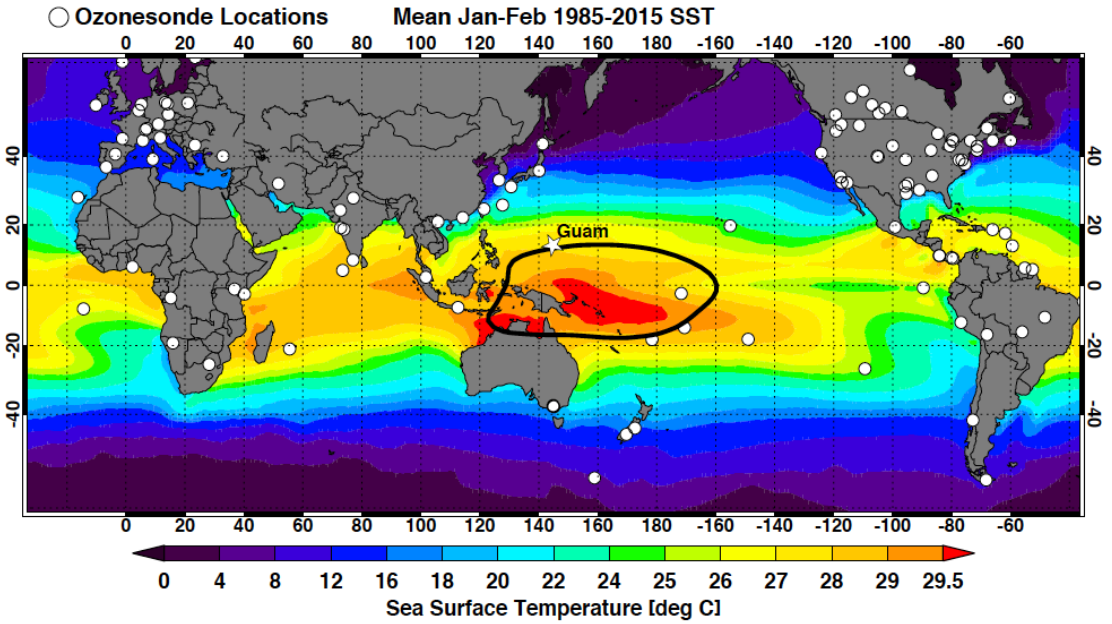

Figure 1. Thirty-year climatology of January-February sea surface temperature (SST), highlighting the TWP warm pool. The SST, shown by the color shaded contours, is from NOAA Optimum Interpolation data version 2 (Reynolds et al., 2002). The 30-year mean 193 K temperature contour at the 100 hPa pressure level (black contour) is shown to indicate the coldest region of TTL. Also shown are locations of ozonesonde measurements (white circles) obtained from WOUDC (http://woudc.org/home.php), which include the SHADOZ stations.

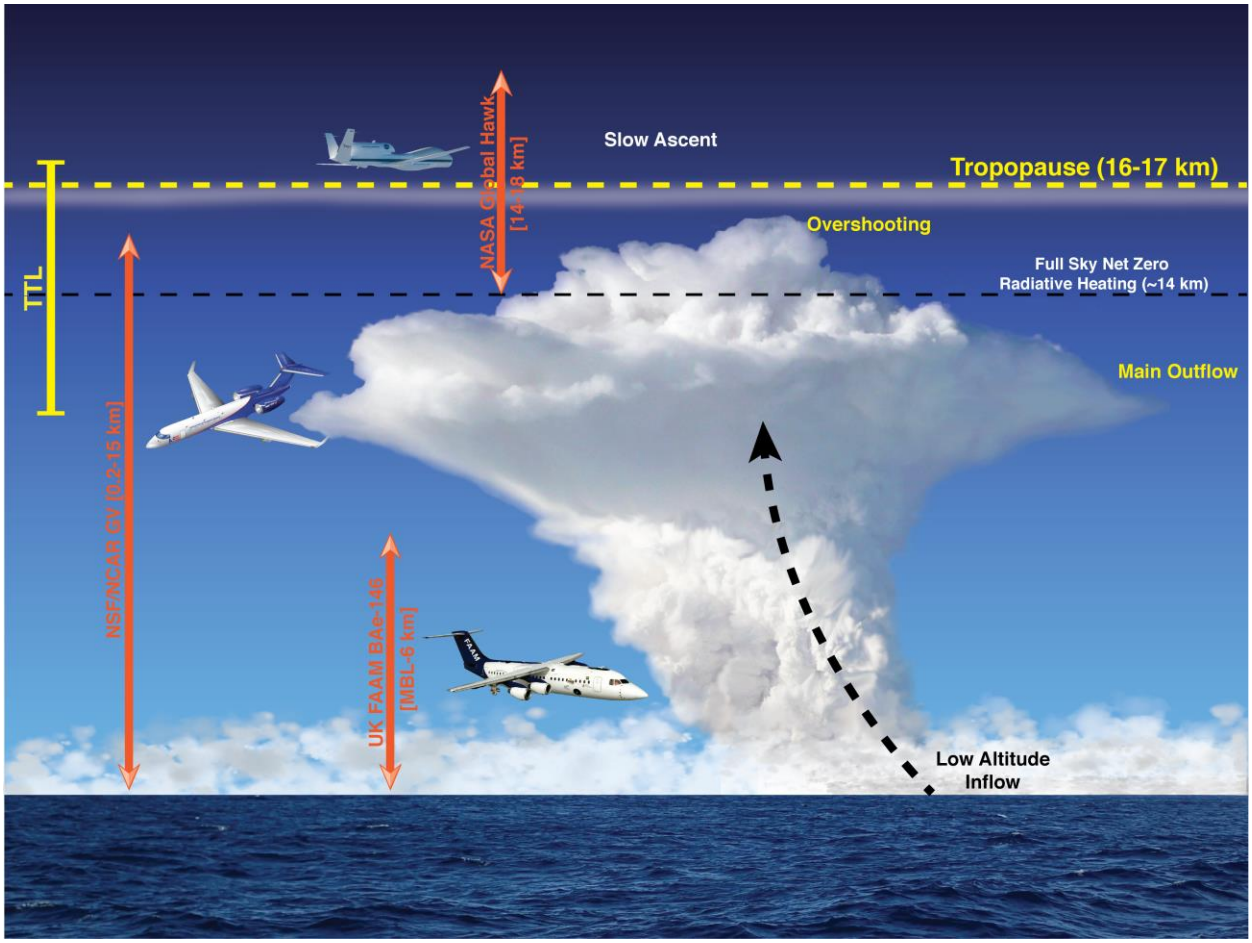

962

963 **Figure 2.** Concept of the coordinated campaigns. This schematic highlights the three
964 research aircraft and the altitude ranges of their sampling in relation to the dynamical
965 background. The key feature of the background is deep convection that nearly reaches the
966 tropopause and which pumps marine boundary layer air into the TTL (~13-17 km). The
967 level of full-sky net zero radiative heating, estimated to be near 14 km, is typically used to
968 indicate the transition into mean upward motion driven by large-scale dynamical control
969 (Corti et al., 2005).

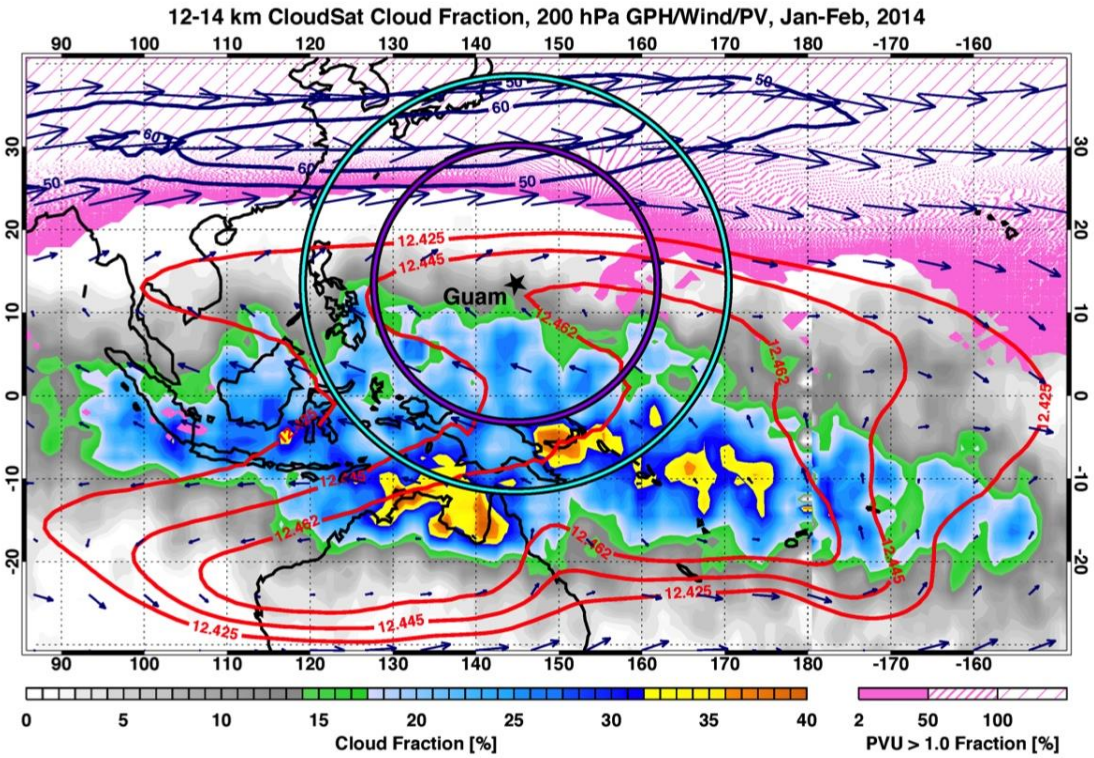

Figure 3. Some key UTLS dynamical elements of the TWP during the CONTRAST campaign period. The figure shows the campaign domain, centered at Guam. The magenta and cyan circles indicate the nominal GV flight range (1000 and 1500 nmi radius respectively). The gray-blue-yellow-orange shading shows the 12-14 km cloud fractions calculated using the CloudSat data, indicating the region dominated by frequent deep convection. The pink stipple shading shows the frequency of 200 hPa PV>1 PVU (1 PVU = 10^{-6} m^{-2} K s^{-1} kg^{-1}) during the campaign period, based on the GFS analyses. The increase in this frequency of PV>1 PVU indicates the transition from the tropics to extratropics. The red contours are selected 200 hPa geopotential height (GPH, in km) levels indicating the region under the influence of mean anticyclonic circulation (Dima and Wallace, 2007). Blue arrows show the 200 hPa wind field; the 50 and 60 m/s wind speed contours are used to indicate the seasonal mean location of the northern hemispheric subtropical jet.

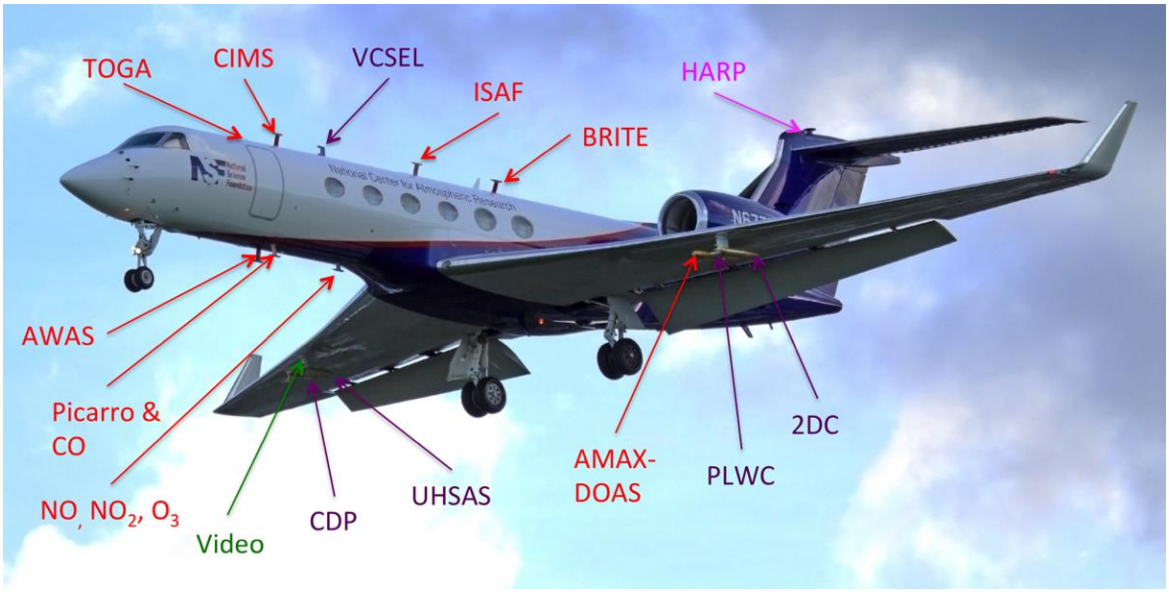

Figure 4. CONTRAST GV payload configuration. See Table 1 for instrument details. The cabin instruments are shown by their inlet locations (with exception of TOGA, its inlet was behind the fuselage in this takeoff photo). The colors are used to indicate the instrument type: chemistry (red), microphysics (purple), radiation (magenta), and the digital camera (green).

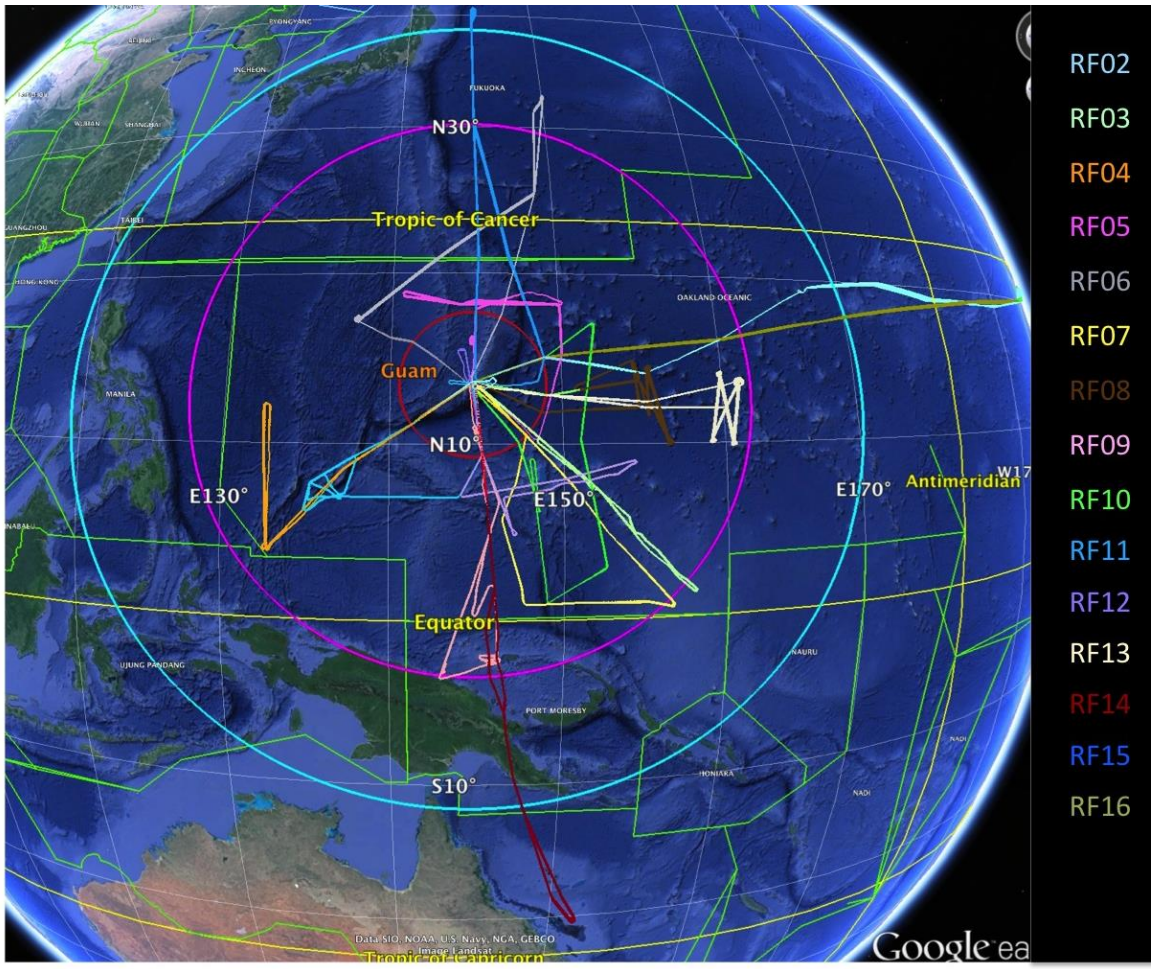

Figure 5. CONTRAST flight operation domain and the GV flight tracks (RF02-RF16). The operational domain is marked by the magenta and cyan circles, which indicate the nominal GV flight range with or without extensive profiling (1000 and 1500 nmi radius respectively). The red ring close to Guam indicates the region covered by the Guam ATC radar. The green lines mark the boundaries of Flight Information Regions (FIRs). As shown, most of the GV flights were operated within the Oakland Oceanic FIR (USA). Three additional FIRs flown were Fukuoka (JPN), Port Moresby (PNG), and Brisbane (AUS).

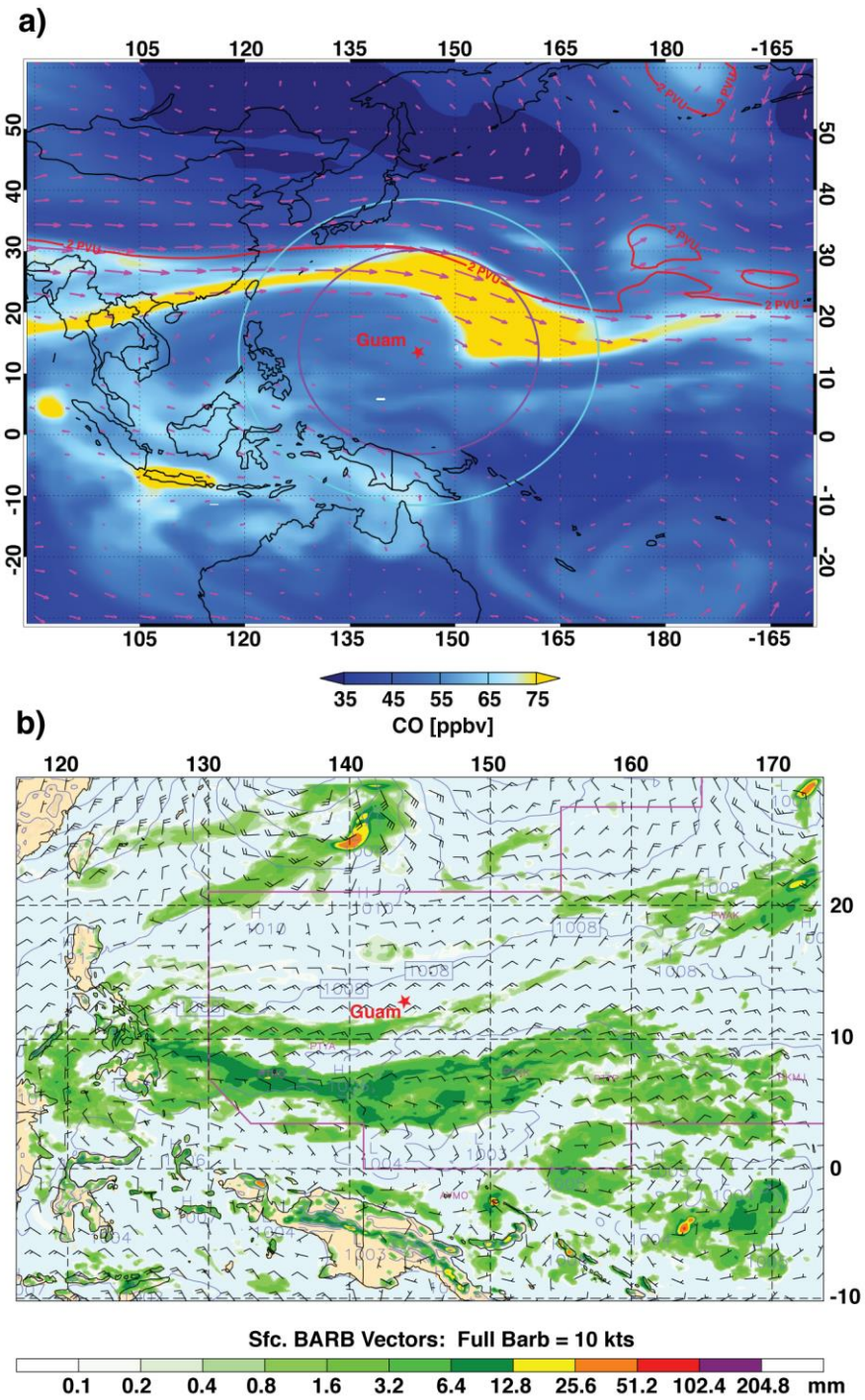

1004

1005 **Figure 6**. Examples of operational weather and chemical forecast plots for RF10 (flight day
1006 8 February 2014). a) CAM-chem-SD 200 hPa CO (color shade) and wind field (pink arrows)
1007 forecast that shows an intense CO plume moving into the Guam domain following the jet
1008 stream. Also shown is the 2 PVU contour at 200 hPa, which marks the division of tropical
1009 UT and extratropical LS. b) The WRF forecast of surface wind (wind barb vectors) and

precipitating convection (shaded), which predicts an ITCZ near 7°N indicated by the surface wind convergence and the line of convection.

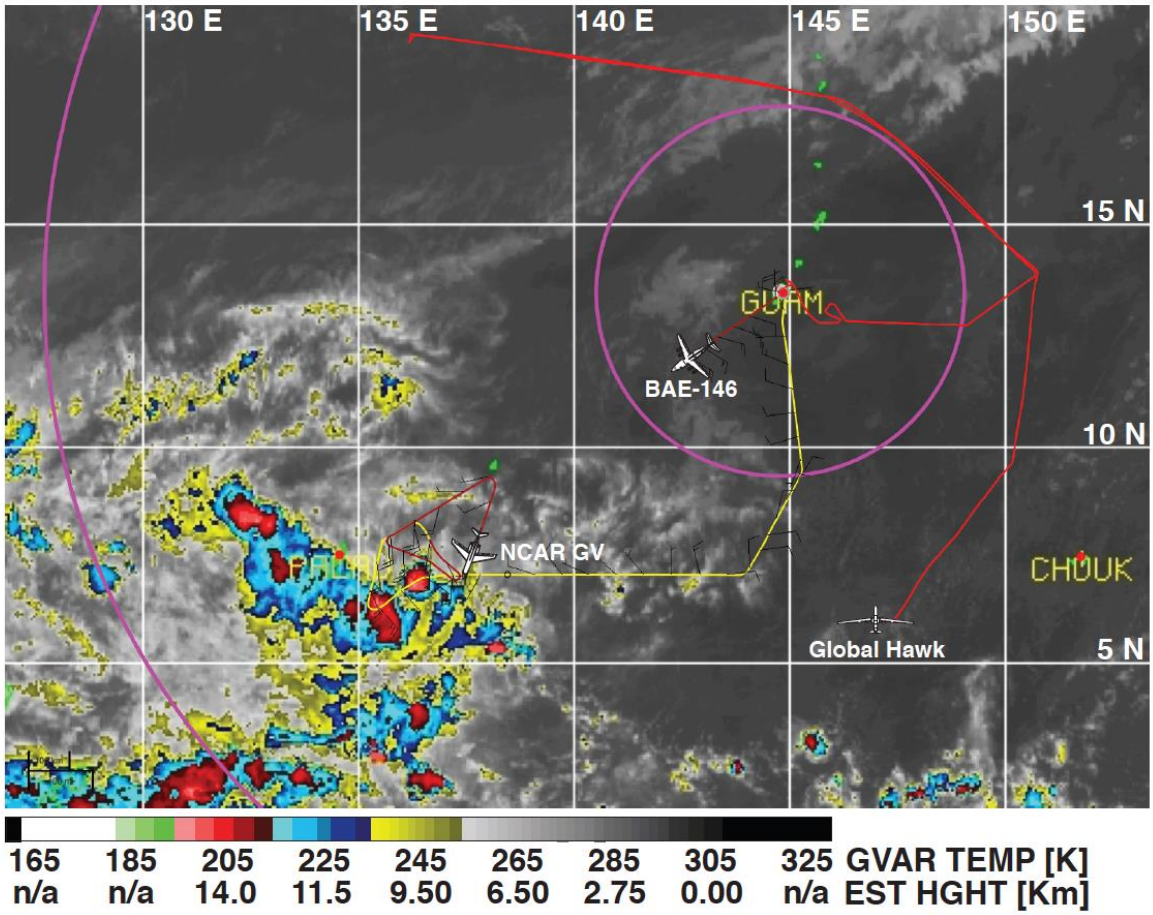

Figure 7. An example of a coordinated flight and the GV targeting active convection. This figure shows the real-time display from the Catalog Map on 13 Feb 2014 near 0400 UTC, around the time the GV sampled the region of convective outflow (see Figure 8). Active convection was widespread southwest of Guam, as revealed by the MTSAT IR (color shading) and visible (gray) channels. The yellow and red lines show flight tracks for each of the three aircraft (red indicates the track for the last hour).

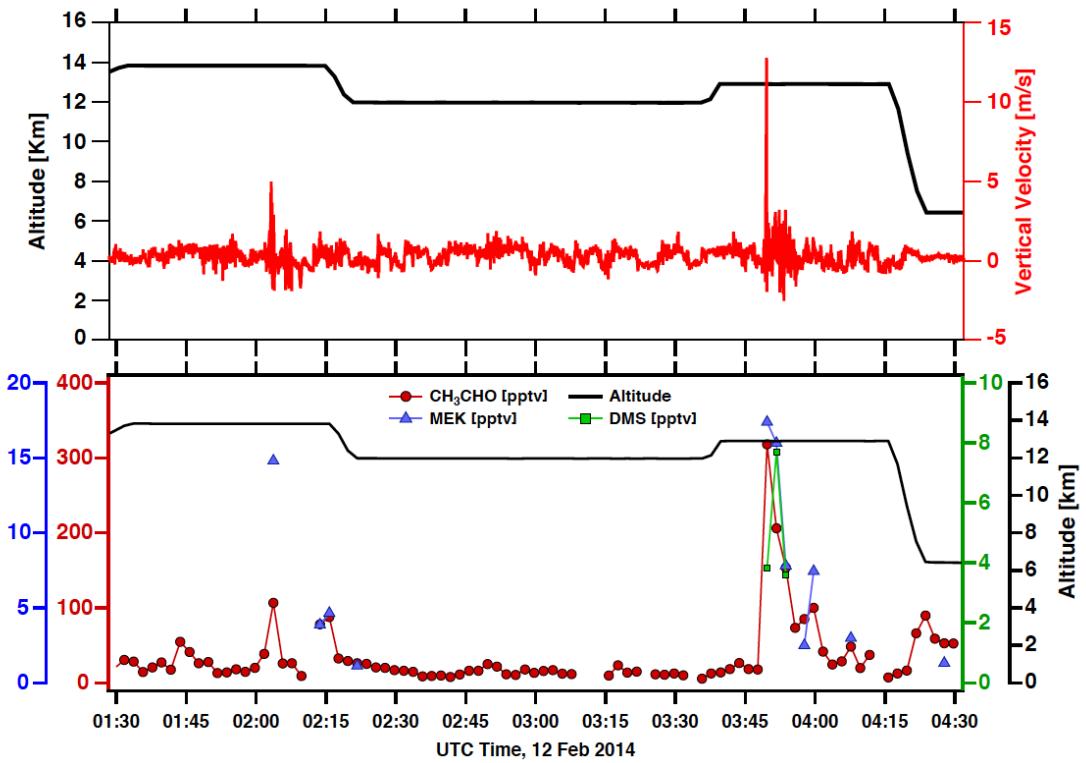

Figure 8. Time series of flight altitudes, vertical velocity, and mixing ratios of selected short-lived compounds during a 3-hour segment of RF11 (12 February 2014) when the GV was targeting the outflow from active convection (see GV location and the region of active convection during this time period in Fig. 7). The active convection regions are indicated by increases in updraft velocity (~ 5 m/s and 13 m/s, respectively). For the aircraft location and the convection, see Fig. 7, which shows satellite IR channel near 04:00 UTC. As indicated by the track in Fig. 7, the GV repeatedly targeted the convective region at different altitudes. The two time periods of successful sampling of fresh outflow (associated with the updraft velocity 5 m/s and 13 m/s) the GV was at 43 Kft (~ 14 km) and 40 Kft (~11 km), respectively. The location of the updraft was in the vicinity of the aircraft position shown in Fig. 7. The tropopause was at ~17 km. The corresponding enhancements of short-lived species in the UT are shown using TOGA observations of acetaldehyde (CH_3CHO), methyl ethyl ketone (MEK; $CH_3C(O)CH_2CH_3$), and dimethyl sulfide (DMS; CH_3SCH_3). DMS and MEK are below the detection limit (1 pptv) for the majority of the UT time segment with the exception of the updraft region, especially during 03:49 - 03:54 UTC.

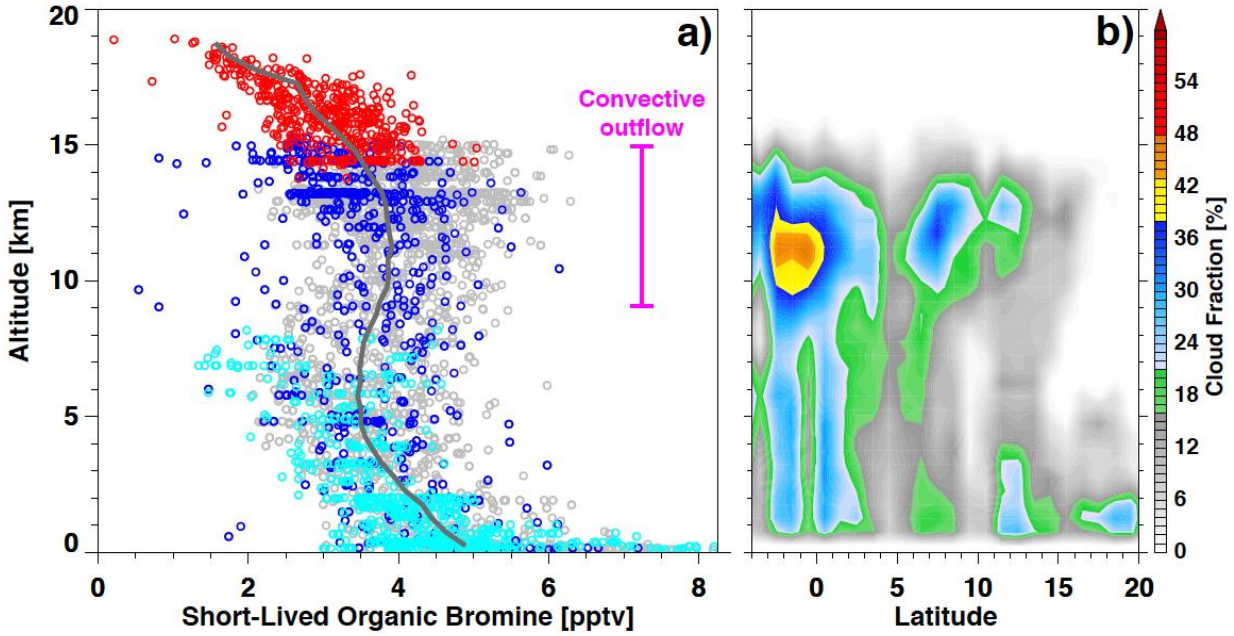

1041

1042 **Figure 9**. (a) Vertical distribution of the total bromine content from two short-lived
1043 organic bromocarbons (2x CH_2Br_2 + 3x$CHBr_3$) from GV TOGA (gray) and whole air
1044 samplers on all three aircraft (Cyan: BAe146, Blue: GV, Red: Global Hawk). The gray line
1045 represents the median profile derived using all four data sets. (b) Latitude-height cross-
1046 section of the mean cloud fraction of the region (140° and 150° E) during the period of the
1047 CONTRAST campaign, calculated using CloudSat satellite data.

1048

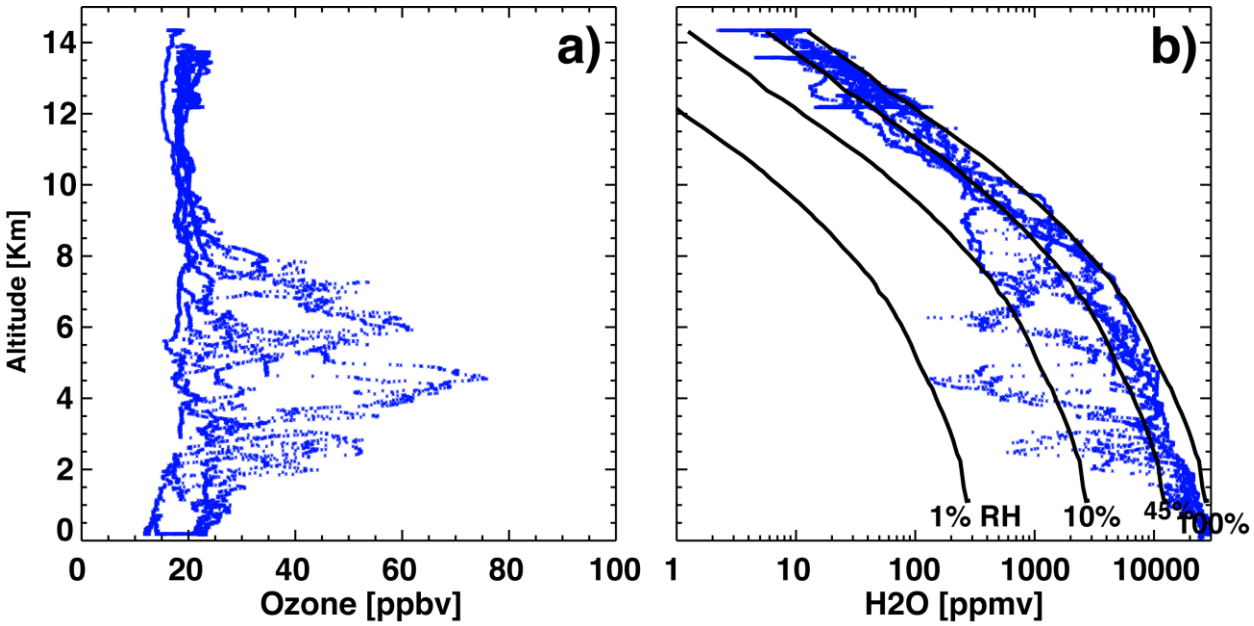

Figure 10. Ozone (a) and water vapor (b) data from RF04, as an example of the ozone profile structure, with layers of ozone enhancement that are coincident with layers of water vapor reduction. Relative humidity (RH) levels corresponding to the measured water vapor and temperature are also shown (black curves).

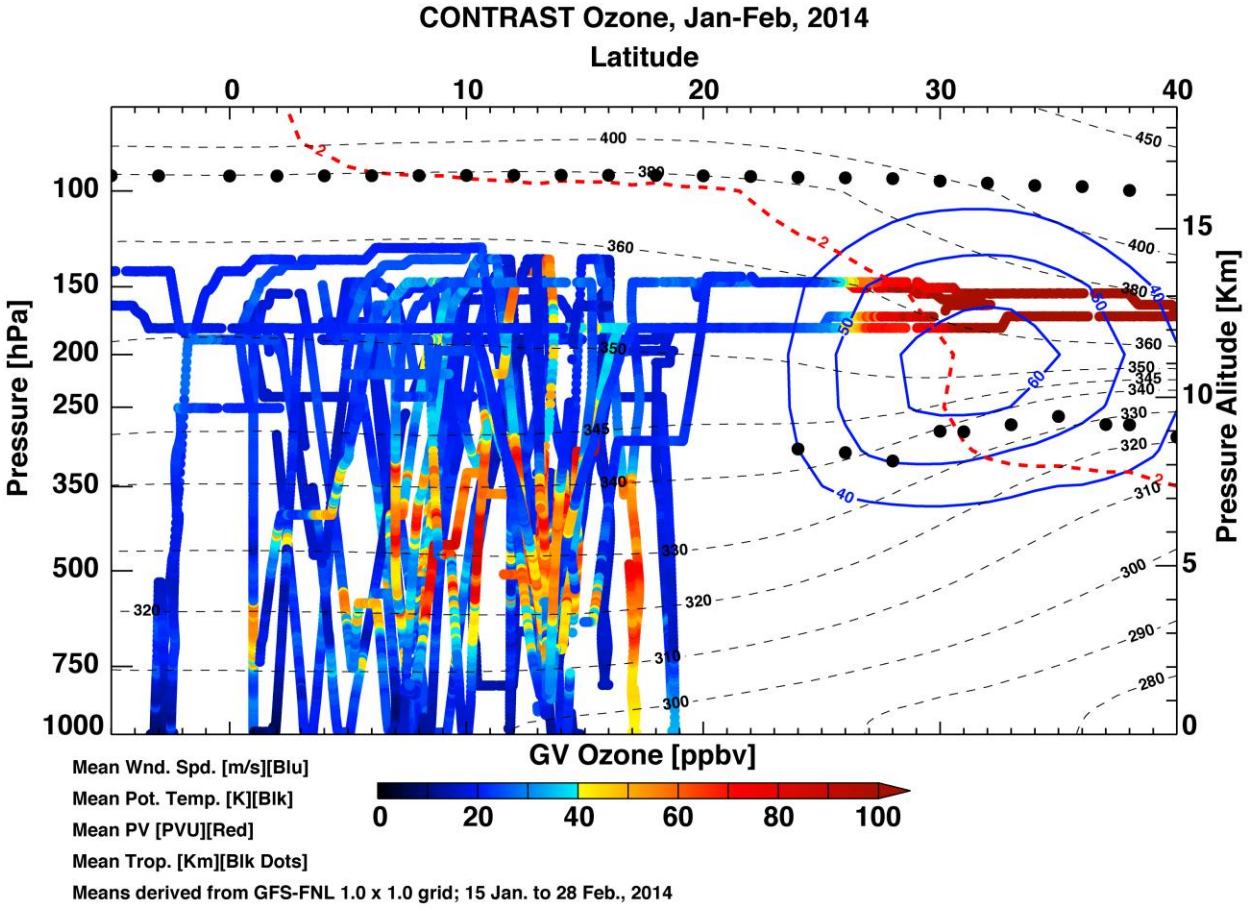

Figure 11. The GV flight tracks for all flights colored by the O_3 mixing ratio. Also included are mean large-scale dynamical structures of the campaign period and domain, represented by the tropopause height (black dots), 2 PVU contour (red dash), subtropical jet location (40, 50, 60 m/s horizontal wind, blue contour) and mean isentropes, all given in sectional zonal mean for 130°-160° E longitude range.

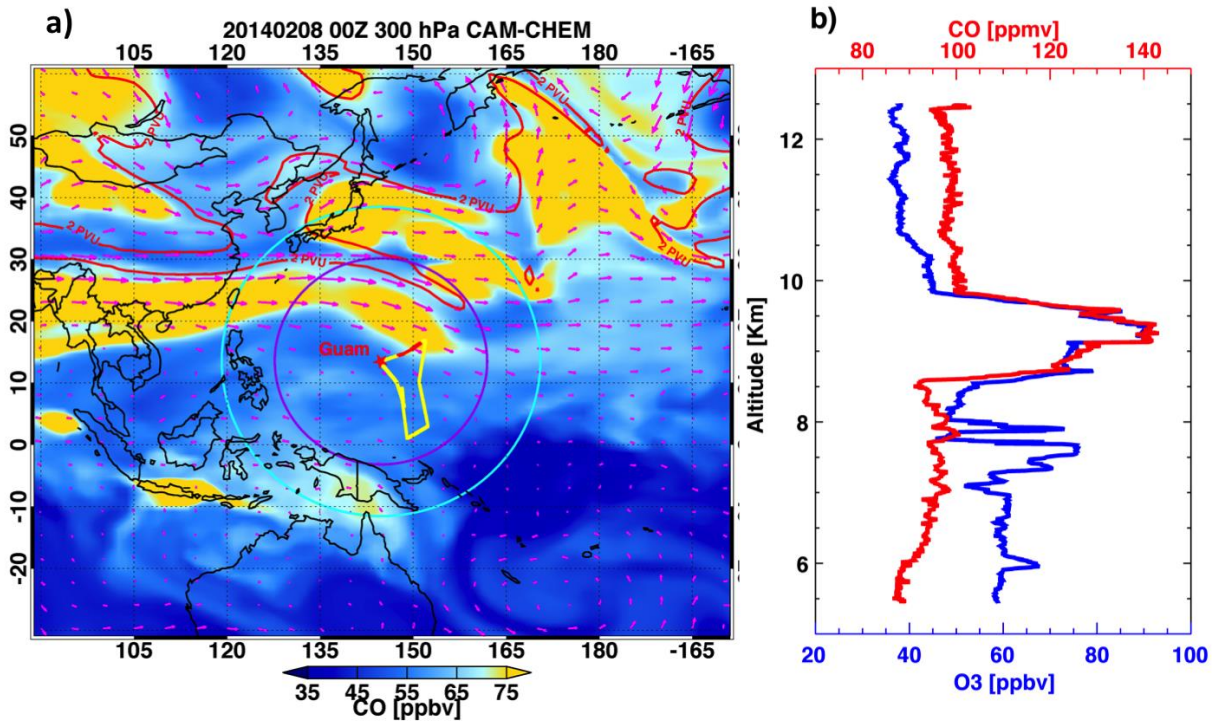

Figure 12. (a) CAM-chem-SD model simulation of CO at the 300 hPa level as well as the aircraft flight track (yellow) and (b) the GV measurements of CO and O_3 in the "CO river" during RF10 on 8 February 2014. The portion of the flight track corresponding to the in situ profile shown in (b) is marked in red on the map (a). The maximum CO enhancement is shown to be ~ 8.5 km altitude (~ 300hPa pressure level).

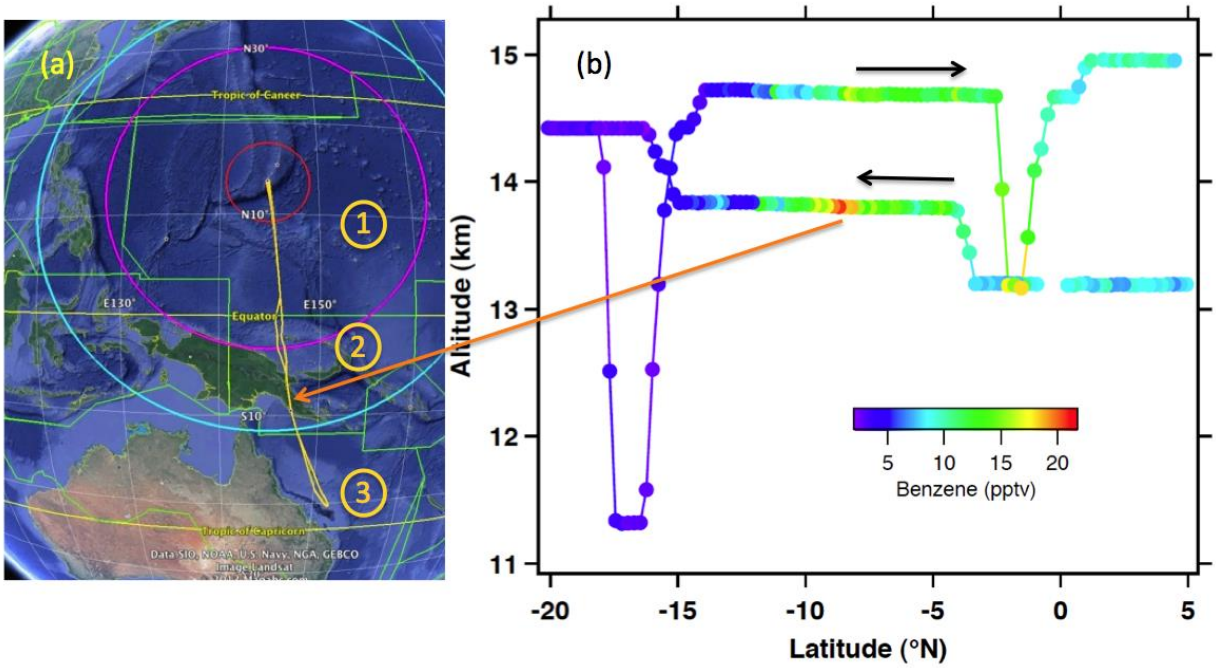

1075

1076 **Figure 13.** Chemical gradients at the TTL level shown by TOGA Benzene data from RF14
1077 flight on 22 February 2014. (a) The flight track shows the large latitude range (~15 ° N –
1078 20°S) sampled. The flight was conducted in three FIRs: 1) Oakland Oceanic (USA), 2) Port
1079 Moresby (PNG) and 3) Brisbane (AUS). (b) Benzene mixing ratio from TOGA highlights the
1080 strong contrast of air over PNG (~8°S) and the Coral Sea (south of 10°S). The black arrows
1081 above the tracks indicate the outbound/inbound flight directions.

1082

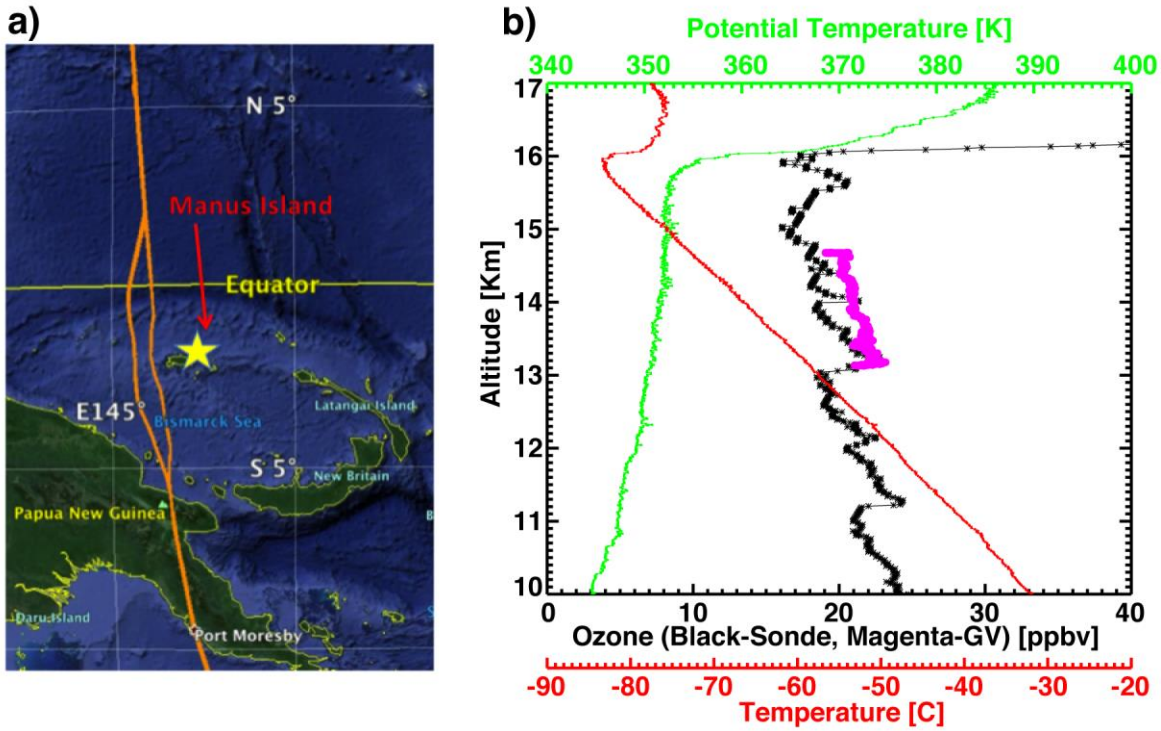

1083

1084 **Figure 14**. (a) GV-ozonesonde coordinated flight during RF14, 22 February 2014 with
1085 Manus Island ozonesonde launch. GV flight track is shown in orange on the map. (b) GV in
1086 situ ozone, sampled during a dip from west of Manus Island from 45 Kft to 41 Kft, is shown
1087 in magenta, while ozonesonde measurements of ozone (black), temperature (red) and
1088 potential temperature (green) are also shown.

1089

1090

1091

Table 1. Payload Summary

Instruments	Measurements	Investigater
Chemistry		
NO_x	NO, NO_2	Weinheimer/NCAR ACD
Fast Ozone	O_3	Weinheimer/NCAR ACD
VUV Carbon Monoxide	CO	Campos/NCAR ACD
Picarro	CO_2, CH_4	Flocke/NCAR ACD
TOGA	NMHCs, OVOCs	Apel/NCAR ACD & Riemer /U. Miami
GT-CIMS	BrO, BrCl, HOBr, ClO	Huey/GIT
AMAX	BrO, IO, H_2CO (remote)	Volkamer/CU
HAIS Advanced Whole Air Sampler (AWAS)	Trace gases	Atlas/U.Miami
In Situ Airborne Formaldehyde (ISAF)	H_2CO	Hanisco/ NASA GSFC
Inorganic Br	Br* (Σ BrO + Br)	Atlas/U.Miami & Flocke/ACD
Radiation		
HARP	Spectral Actinic Flux	Hall /NCAR ACD
State parameters		
State Parameters	Lat/Lon, P, T, 3D wind	Jensen/NCAR RAF
RAF Digital Video	Fwd view	Jensen/NCAR RAF
Microphysics		
CDP Cloud Probe	2 - 50 um, water droplets, ice crystals	Jensen/NCAR RAF
2D-C Precipitation Probe	25-1600 um, ice, water	Jensen/NCAR RAF
UHSAS Aerosol Probe	0.075 - 1 um, aerosols	Jensen/NCAR RAF
WCN CN Counter	0.01 - 3 um, aerosols	Jensen/NCAR RAF
VCSEL Laser Hygrometer	water vapor	Jensen/NCAR RAF

1092

1093

Table 2. Research Flight Summary

Flight	Date	Flight Type, Scenario #	Flight Region
RF01	11-Jan-2014	Research transit, 1	Colorado to Hawaii
RF02	13-Jan-2014	Research transit, 1	Hawaii to Guam
RF03	17-Jan-2014	Domain survey, 1	Guam to SE (Chuuk)
RF04	19-Jan-2014	Domain survey, 1	Guam to SW (Palau)
RF05	22-Jan-2014	Convective outflow, 2	North of Guam
RF06	24-Jan-2014	Jet crossing/pre-post frontal contrast, 4, 5	North and Northwest of Guam, entering Fukuoka FIR (JPN)
RF07	29-Jan-2014	SH convective outflow survey, 1, 4	Guam to equatorial region
RF08	1-Feb-2014	Photochemical evolution - sunset, 3, 7	Guam to East (the stagnation point in the anticyclone)
RF09	4-Feb-2014	Equatorial crossing and Manus ozonesonde, 2, 6	Guam to Port Moresby FIR (PNG)
RF10	8-Feb-2014	Subtropical jet pollution and ITCZ survey, 2,5	Guam to near equator crossing ITCZ near 6°N
RF11	12-Feb-2014	Convective outflow and coordinate flight, 2, 6, 7	Guam to south and southwest
RF12	17-Feb-2014	Convective outflow and coordinated flight, 2, 6, 7	Guam to south and southeast
RF13	19-Feb-2014	Photochemical evolution - sunrise, 3	Guam to East (the stagnation point of the anticyclone)
RF14	22-Feb-2014	Equator crossing, SH TTL survey, and Manus ozonesonde, 1, 2, 6	Guam to Port Moresby FIR (PNG) & Brisbane FIR (AUS)
RF15	24-Feb-2014	Jet crossing and lower stratosphere survey, 4	Guam to 40°N Fukuoka FIR (JPN)
RF16	28-Feb-2014	Transit flight with limited research, 1	Guam to Honolulu